DC-ELECTROKINETIC MOTION OF COLLOIDAL CYLINDER(S) IN THE VICINITY OF A WALL

A THESIS SUBMITTED TO

THE GRADUATE SCHOOL OF ENGINEERING AND SCIENCE

OF BILKENT UNIVERSITY

IN PARTIAL FULFILLMENT OF THE REQUIREMENTS FOR

THE DEGREE OF

MASTER OF SCIENCE

IN

MECHANICAL ENGINEERING

By

Atakan Atay

July 2021

DC-electrokinetic motion of colloidal cylinder(s) in the vicinity of a wall
By Atakan Atay
July 2021

We certify that we have read this thesis and that in our opinion it is fully adequate, in scope and in quality, as a thesis for the degree of Master of Science.

Barbaros Çetin(Advisor)

Ali Beşkök

Ender Yıldırım

Approved for the Graduate School of Engineering and Science:

Ezhan Karaşan
Director of the Graduate School

ABSTRACT

DC-ELECTROKINETIC MOTION OF COLLOIDAL CYLINDER(S) IN THE VICINITY OF A WALL

Atakan Atay
M.S. in Mechanical Engineering
Advisor: Barbaros Çetin
July 2021

DC-electrokinetic behavior of colloidal particles in the vicinity of a conducting/non-conducting planar boundary is investigated using an inhouse boundary element method (BEM) based solver in MATLAB® environment. In the model, contribution of hydrodynamic drag, electrokinetic (electrophoretic and dielectrophoretic), and colloidal forces (van der Waals and EDL) to over-all particle velocity is computed. The electrokinetic and colloidal forces are calculated using prescribed relations obtained from the literature. These forces are then included in the model as external forces acting on the particles. The electrokinetic (EK) forces are obtained by integrating Maxwell stress tensor (MST) over particles' surfaces. Throughout this work, a thin EDL assumption is made. Position and velocities of the particles along with resulting flow and electric fields are computed. Overall, results are compared with experimental observations and a general discussion regarding colloidal behavior is made.

Keywords: Microfluidics, boundary element method, colloidal cylinder.

ÖZET

KOLLOİD SİLİNDİRLERİN DUVAR KENARINDAKİ DC ELEKTROKİNETİK HAREKETİ

Atakan Atay
Makine Mühendisliği, Yüksek Lisans
Tez Danışmanı: Doç Dr. Barbaros Çetin
Temmuz 2021

Duvar kenarındaki kolloid parçacıkların doğru elektrik alan altındaki elektrokinetik hareketlerinin incelenmesi için MATLAB® ortamında sınır eleman (BEM) yöntemine dayalı bir formülasyon geliştirilmiştir. Hidrodinamik sürüklenme, yer çekimi, elektrokinetik (elektroforetik ve dielektroforetik) ve kolloidal (van der Waals ve Elektriksel Çift Katman) kuvvetlerin etkileri modele dahil edilmiştir. Elektrokinetik ve kolloidal kuvvetlerin hesabı için literatürdeki denklemlerden yararlanılmıştır. Bahsi geçen kuvvetler parçacık hareketini etkileyen dışsal kuvvetler olarak formülasyona eklenmiştir. Parçacık üzerine etkiyen elektrokinetik kuvvet değeri, parçacık yüzeyi boyunca maxwell stress tensörü (MST) integralinin hesaplanması ile elde edilmiştir. Simülasyonlarda duvar ve parçacık yüzeylerinde elektrokinetik kayma hızı ve ince elektriksel çift tabaka (EDL) varsayımları yapılmıştır. Simülasyonlar sonucunda parçacıkların hız ve konumları ile elektrik alan ve akış bölgeleri elde edilmiş, duvar kenarındaki kolloid parçacıkların duvar kenarındaki elektrokinetik davranışları literatürdeki deneysel veriler ışığında incelenmiştir.

Anahtar sözcükler: Mikroakışkanlar, sınır eleman metodu, kolloid silindir.

Acknowledgement

I would like to express my gratitude to my principal advisor Assoc. Prof. Dr. Barbaros Çetin for his continued guidance throughout my academic journey. Among many other things, he helped me grasp the bigger picture whenever I got lost at the details. I am also grateful to him for taking a note of my opinions and making me feel like one of his colleagues rather than a mere student during our discussions.

Many thanks to Prof. Dr. Ali Beşkök for his valuable contributions and his precious guidance. It is with his support that I am able to interpret the results and present them in a meaningful form. I am grateful for the opportunity of meeting him in person.

I would like to express my appreciation to Assoc. Prof. Müjdat Tohumcu, Assoc. Prof. Dr. Ender Yıldırım, Asst. Prof. Dr. Luca Biancofiore and Assoc. Prof. of Mech. Eng. Dr. Yiğit Akkuş for their support during my application period. They stood by my side during tough and uncertain times.

I would like to thank all my valuable fellow researchers Mehmet Akif Şahin, Alper Topuz, Büşra Sarıarslan, Hande Nur Açıkgöz, Alara Karaman, Osman Berkay Şahinoğlu, Burak Sarı, Berke Demiralp, Emre Eraslan, Berk Küçükoğlu, Mehmet Kelleci, Kaan Karaca, Didem Fatma Demir, Tufan Erdoğan, Ali Yücel and Görkem Balyalıgil for all bright memories we had together. I genuinely thank them for valuable discussions we made and pleasant memories we had. Their presence provided moral support.

Last but not least, I wholeheartedly thank my family. This thesis would not come to an end if I did not have their full support.

Contents

1 Introduction **1**

1.1 Theory 1

1.1.1 Electrokinetics 1

1.1.2 Modeling of Particle Motion 7

1.2 Objectives and Motivation 14

1.3 Thesis Outline 14

2 Boundary Element Formulation **16**

2.1 Fluid Flow Model 16

2.2 Electrical Field Model 18

2.3 Particle Tracking 20

2.4 Algorithm of the Solver 22

3 Validation of the Model **24**

3.1 Hydrodynamic Benchmarks 25

3.1.1 Drag Force on a Particle next to a Single Wall 25

3.1.2 Drag Force on a Particle Between Two Walls 26

3.1.3 Pressure Validation In Domain 28

3.2 Electrokinetic Benchmarks 29

3.2.1 Electric Field Parallel to a Wall 29

3.2.2 Electric Field Perpendicular to Wall 31

3.2.3 Validation of Electric Field 32

4 EK Motion of Colloidal Cylinder(s) 33

4.1 Conducting Wall 33

4.2 Non-Conducting Wall 42

5 Conclusion and Future Work 50

A Calculation of DEP Force 59

B Evaluation of Singular Integrals 61

C Boundary Conditions 63

C.1 Conducting Wall 63

C.2 Non-Conducting Wall 64

D Convergence of the Solver 66

E Code **67**

List of Figures

1.1 Schematics of Electric Double Layer (EDL) 2

2.1 Flow chart of the custom algorithm used in present study 23

3.1 Schematics of hydrodynamic benchmark with a single wall 25

3.2 Schematics of hydrodynamic benchmark with a double wall 27

3.3 Schematics of the benchmark problem for pressure 28

3.4 Schematics of the EK benchmark problem near a conducting wall 29

3.5 a: Comparison of non-dimensional horizontal velocity b: comparison of non dimensional rotational velocity with respect to analytical solution 30

3.6 a: Schematics of the benchmark problem near a conducting wall, b: Comparison of non-dimensional velocity between present study and analytical solution 31

3.7 a: Non-dimensional potential distribution in the domain, b: Non-dimensional electric field comparison in a square domain 32

4.1 Comparison of the present study with the analytical solution given by Wang and Keh for the case of single particle near a conducting wall with Dirichlet boundary condition, and the result of the present study with the Neumann boundary condition. 34

4.2 The position and velocity of a particle in the y–direction as it moves towards the wall. The contributions of different physical phenomena on the velocity are shown separately. 36

4.3 Flow and electrical fields around a particle as it moves towards the wall. Electric field lines and the streamlines are shown. Background color corresponds to non-dimensional electric potential and non-dimensional pressure distribution, respectively. The right column shows the non-dimensional wall potential and wall slip-velocity at different times. 37

4.4 Schematic description of multi-particle problem next to a conducting wall 38

4.5 The position and velocity of multiple particles in the y–direction and x–direction as they move towards the wall. The contributions of different physical phenomena on the velocity are shown separately. 39

4.6 Electric field lines and streamlines at three different instances during the two-particle motion. Non-dimensional electric potential and pressure field contours are also shown in the background. The right column shows the non-dimensional potential and slip-velocity on the electrode's surface at three distinct times. 41

4.7 Non-dimensional velocities of a single particle in the vicinity of a non-conducting wall for a particle whose diameter is 15μm. 44

4.8 Schematics of two particle problem near a non-conducting wall . . 45

4.9 Vertical and horizontal velocities of the first particle with a diameter of 15μm 46

4.10 DEP forces in x− and y− directions throughout the simulations for the particles with a diameter of 15μm 46

4.11 Vertical and horizontal velocities of the second particle with a diameter of 15μm 47

4.12 Maxwell Stress Tensor (MST) comparison for the particles in the vicinity of a wall 48

4.13 Maxwell Stress Tensor (MST) comparison for the particles in the vicinity of a wall 48

4.14 Non-dimensional potential and electric field of 15μm particles . . 49

B.1 Non-uniform transformation of Gauss points on the particle boundary for a singular integral 62

D.1 Convergence of the quadratic solver 66

List of Tables

1.1 Summary of the Literature 13

3.1 Comparison of BEM vs analytical solution of drag force acting on a cylindrical object in the vicinity of a single wall 26

3.2 Comparison between present study, Richou *et al.* [54], and analytical solution given by Faxèn *et al.* [54] for the calculation of hydrodynamic drag force acting on a particle between a double wall. 28

3.3 EK velocity comparison between present study (PS), Dustin *et al.* [60] and the analytical solution given by Keh *et al.* [30]. 30

4.1 Velocity components for colloidals with different diameters 44

Chapter 1

Introduction

1.1 Theory

1.1.1 Electrokinetics

EK manipulation of colloidals often come into use in various applications such as field-induced layering of colloidals [1], guided patterning of particles on substrate surfaces as a 2-D and 3-D colloidal structures [2], fabrication of nano devices [3], electrophoretic deposition of colloidal particles [4], local colloidal crystallites [5], planar superlattices of binary colloidal suspensions [6] as well as miniaturized biosensors [7]. An interesting behavior pertaining EK colloidals is that particles possesing charges of same type aggregate under external electrical field despite presence of repulsive coulombic forces. Although there are experimental observations regarding this behavior [1, 8, 9], there is no rigorous model that simulates EK behavior of colloidals in close proximity to a planar wall with a detailed examination of particle-particle (p-p) and particle-wall (p-w) interactions together with the inclusion of colloidal (vdW, EDL) and dielectrophoretic (DEP) forces.

Solid particles posses electrostatic charges on their surface. In general, aqueous solutions are charge-neutral. That is to say, number of positive charges balance

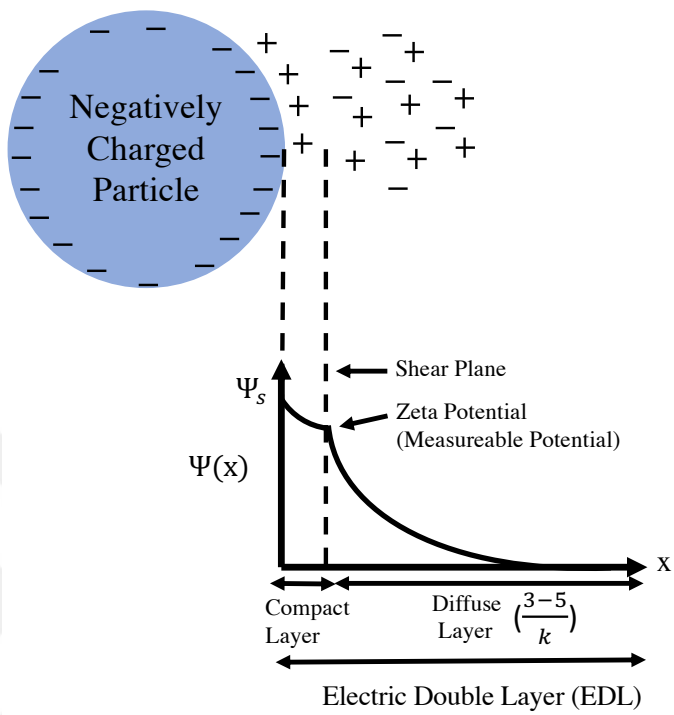

Figure 1.1: Schematics of Electric Double Layer (EDL)

negative charges in the solution. Concerning flows with small Reynolds number such as Stokes flow, the inertial effects in the fluid domain becomes negligible. As a result, once a solid surface comes into contact with an aqueous solution, ions on the solid surface attract counterions and repel coions in the neutral solutions. The counterion concentration in the vicinity of the solid particle in the solution side is larger than that of the bulk. This produces a potential difference on the interface. The charged solid surface and a layer of ions in the vicinity of the charged layer is called Electric Double Layer (EDL). As it is seen in Fig. 1.1, right next to the charged solid surface, there is an immobile layer of ions attracted to the solid surface. The immobile layer is called the *compact layer*. Starting from the compact layer to the electrically neuter bulk liquid, the net charge density gradually decreases to zero. Compared to those at the compact layer, charges in this region are affected much less by the electrostatic interactions and are mobile. This region is called *Diffuse layer*. Diffuse layer together with compact layer form the electric double layer.

Thickness of the electric double layer depends on the several properties of the solution: bulk ionic concentration, temperature of the environment, and electrical properties of the solution. Characteristic EDL length of such structure is represented by inverse of *Debye-Hückel parameter*, $(1/\kappa)$. In general, EDL thickness may vary from several nanometers to few microns depending on the ionic concentration of the solution [10]. For an electrolyte with symmetric ions, κ can be written as:

$$\kappa = \sqrt{\frac{2z^2e^2n_\infty^2}{\varepsilon k_B T}} \tag{1.1}$$

where z is the valence of the ions, e is the elementary charge, n_∞ is the bulk ionic concentration, k_B is Boltzmann's constant, and T is the absolute temperature. Considering conventional fluid mechanics applications where inertial terms are considerably effective on the solution domain, the velocity on shear plane is considered to be zero, which is known as *no-slip* boundary condition. In microfluidics, if the EDL is thin, in order to avoid the rigorous modeling of nm scale EDL, thickness of the EDL is neglected and a slip velocity is assigned on the boundary. Slip velocity is a function of the applied electrical field (E_∞), permittivity of the vacuum (ϵ_o), relative permittivity of the particle (ϵ_r), the zeta potential of the particle and the water (ξ_p, ξ_w) (measureable potential on the surface).

In microfluidic applications, electrokinetic manipulation of colloidals is a necessity [11]. Regarding EK manipulations of colloidals, electrophoresis(EP) and dielectrophoresis (DEP) are two most commonly referred approaches. Once a charged particle is exposed to an external electric field, the particle is going to migrate to either anode or cathode depending on the charge of the particle, which is a well-known phenomenon called electrophoresis (EP) [12]. The electrophoretic behavior of a single particle in an unbounded flow is governed by *Smoluchowski* formula.

$$\mathbf{V_{particle}} = \mathbf{E}_\infty \frac{\epsilon_r \epsilon_o (\zeta_p)}{\mu} \tag{1.2}$$

On the other hand, due to high counterion concentration on the solution side of the interface, water molecules will be dragged to the opposite direction of particle motion. This phenomenon is known as *electroosmosis*. In a typical microfluidic setting, electroosmosis and electrophoresis occur simultaneously. DEP, on the

other hand, is the motion of the dielectric particles due to an inhomogenous electric field around them [13]. In other words, if electrophoresis is described as a tool used to transport particles along microchannel, then DEP could be described as another tool that is often used to create lateral migration of such particles [14]. DEP forces could be realized under externally applied DC and AC electric fields. In order to find total DEP force acting on the particle, one must integrate Maxwell Stress Tensor (MST) over particle's surface.

$$\mathbf{F}_{\mathrm{DEP}} \oint_{\partial\mathcal{D}} \boldsymbol{\sigma}_{\mathrm{MST}} \cdot \mathbf{n} \, d\Gamma \tag{1.3}$$

where Maxwell Stress Tensor is defined to be:

$$\sigma_{\mathrm{MST}} = \varepsilon \mathbf{E} \otimes \mathbf{E} - \frac{1}{2}\varepsilon(\mathbf{E} \cdot \mathbf{E}) \, \mathbf{I} \tag{1.4}$$

Detailed information regarding calculation of DEP force could be found in Appendix A.

In the literature, electrokinetic behavior of colloidals have been widely investigated. However, in microfluidic applications, p-p and p-w interactions are inseparable part of the microfluidic processes. Therefore, numerous theoretical studies in the literature investigated p-p and p-w interactions. Though EK particle motion behavior in an unbounded flow is well-known thanks to Smoluchowski formula, the phenomenon becomes complicated due to presence of other particle/boundaries as external boundaries cause a change in local electric and flow fields around the particle. In some cases, these disturbances in the local field might induce highly non-uniform fields, which in turn may yield a strong DEP force acting on the particle due to presence of the wall [15–20] or due to presence of other proximate particles. In some cases, this is known to cause a chain formation among the particles [20–24]. Furthermore, the presence of particle results in a disturbance in the local field near a conducting wall and such disturbance induces an electro-hydrodynamic (EHD) fluid flow responsible for the lateral migration, perpendicular to the direction of electrical field, yielding aggregation of colloidals which is a phenomenon also observed in experiments [1, 2, 4–6].

Boundary effects owing to altered electric and flow fields aside, if the particles are sufficiently close to each other, they experience repulsive forces due to

Coulombic and dipole-dipole interactions also known as EDL forces and vdW forces. These two forces are called colloidal forces in classical DLVO (Derjaguin-Landau-Verwey-Overbeek) theory [15].

EP motion of a set of spherical particles ranging from a few μm to ten μm in the vicinity of a non-conducting wall with an electric field parallel to the wall was investigated by Keh and Chen [25] via an eigenfunction expansion series with an assumption of thin EDL. Their results reveal that as the gap between the wall and the particle decreased, the translational and angular velocities of the particle enhanced.

For the same problem, particle in the vicinity of a non-conducting wall, Yariv and Brenner [26] employed a matched asymptotic expansion to understand the dynamics of the EP behavior of the particle for the gap distances smaller than 5% of the particle diameter. They showed that translational and angular velocities of the particle further enhance in near-contact. Ristenpart *et al.* [27], theoretically modelled the EK flow around a spherical particle in close proximity to a conducting wall under a steady electric field including Faradaic current and surface conduction. These phenomena become prominent as zeta potentials on the particle surfaces are of same order of magnitude with thermal voltages. They derived a closed-fomr solution in thind EDL and slow Faradaic reactions and discussed induced EK flow around the particle by indicating specific contributions of electro-osmosis and EHD. With an approximation of Faxèn's law, they discussed aggregation of two particles by solving for the the flow field of induced by other particle. Ristenpart *et al.* [28] also developed a model for an oscillatory electric field. Yariv [29] investigated the same problem in the near-contact.

One of the leading works regarding EK behavior of the particles in 2-D is carried out by Keh *et al.* [30] who solved the EP of a cylindrical particle with an electric field parallel to a non-conducting wall and normal to a conducting wall in the thin EDL limit. They reported that for the case of cylinder, the EK behavior is similiar to that of sphere's. As opposed to non-conducting wall, results for an electric field normal to a conducting wall yielded zero angular velocity for a single particle due to symmetricity in electric and flow field around the particle. It was

also found that next to a conducting wall, vortice formation was induced. Once again, Yariv [18] employed matched asymptotic expansion for the electrophoresis of a cylinder in near-contact limit. However, in this work, he included DEP contribution and reported that DEP contribution was a dominant factor on the equilibrium distance of the particle in a setting in which electric field is parallel to a non-conducting wall. However, DEP on equilibrium location was found to be negligible in the vicinity of a conducting wall.

Wang and Keh [31] extended their previous study [30] to incorporate the effect of thin but polarized EDL and corrected their previous results for a conducting wall in the thin EDL limit. Yariv [19] analyzed the EP of a spherical particle near a non-conducting wall with an electric field parallel to the wall incorporating DEP and surface conduction on the solid boundaries. The results revealed that surface conduction effectively reduces the significance of the locally disturbed field, and hence, the DEP contribution. For the same problem, Young and Li [15] investigated the equilibrium position of a particle normal to a wall in the presence of DEP and colloidal forces. The DEP contribution was calculated by determining the local electric field and the integration of the Maxwell stress tensor around the particle, and the colloidal forces were included by implementing readily available force expressions available in the literature. The findings showed that the equilibrium position of a particle was affected by the DEP and colloidal forces, and the omission of DEP contribution may result in underestimation of the equilibrium position of the particle. Camarda *et al.* [17] studied EK motion of spherical particles and identified a region in the close vicinity of a conducting wall in which cohesive and repulsive forces (in contrast to what is predicted by ignoring any particle-wall interaction) are generated on the particle due to the particle-wall interactions. Later Cetin *et. al* [20] also demonstrated this effect within microchannel confinements.

Concerning settings in which a particle is in the vicinity of an electrode (i.e. a conducting surface), chemical properties of the surfaces gain prominance. In addition, the presence of the particle creates a disturbance in the distribution of electric potential on the electrode and yields an EHD flow [27, 28, 32–34]. Determination of potential distribution on the wall is beneficial for the investigation

of the flow field between particle and the electrode. It is possible to assign a constant potential value along the electrode surface (i.e. Dirichlet B.C.) for a high frequency oscillatory fields without any Faradaic reactions [17,18,20,27–29]. However, such boundary condition on electrode results in omission of EK slip on the conducting wall and prevents EHD flow from occuring. Whereas, a current density on an electrode (i.e. gradient of electric potential which is equal to the emitted electric field form wall) results in EK slip due to induced electric field owing to the presence of the particle , which means the electrochemical properties of the electrode are related to the current density with applied voltage. However, Ristenpart *et al.* [27] used a non-homogenous Neumann condition to capture EHD flow based aggregation of particles which could be quite appropriate for relatively weak electric fields (< 0.6 V/cm) [33,34]. Though cornerstone studies involving DC electric field set constant potential on electrode surface for the sake of computational simplicity [25,30,31,35], application of a current density based boundary condition (i.e. Neumann boundary condition) on the electrode surface is a more realistic approach to capture flow dynamics of colloids in the vicinity of a conducting wall [27–29,33,34].

1.1.2 Modeling of Particle Motion

Microfluidic processes inherently involve p-w and p-p interactions, which introduce complexity to the prediction of the EK behavior of colloidals. There is no analytical solution for multibody interactions in the vicinity of a boundary. However, with a proper choice of numerical method, this complexity could be overcome. Methods for particle tracking could be categorized under two different approaches: point-particle approach, and finite-sized particle approach. In the first case, it is assumed that (i) particle's rotation does not affect its trajectory, (ii) p-p electrostatic interactions could be ignored. In point particle approach, also known as Lagrangian Particle Tracking methods (LTM), $\mathbf{x_p}$ could be predicted with the following approach:

$$\mathbf{x}_\mathrm{p} = \mathbf{x}_\mathrm{o} + \int_0^\mathrm{t} \mathbf{u}_\mathrm{p}(\mathrm{t}')\mathrm{dt}' \tag{1.5}$$

where $\mathbf{x}_o$ is the initial location of the particle and $\mathbf{u}_p$ is the particle velocity. For an inertial reference of frame, translational motion of a particle is governed by the following differential equation:

$$m_p \frac{d\mathbf{u}_p}{dt} = \mathbf{F}_{ext} = \mathbf{F}_{DEP} + \mathbf{F}_{EK} + \mathbf{F}_{Col} \tag{1.6}$$

where m_p is the particle mass, $\mathbf{F}_{ext}$ is the external forces such as hydrodynamic force, $\mathbf{F}_H$, DEP force, $\mathbf{F}_{DEP}$, colloidal forces, $\mathbf{F}_{COL}$. In LTM methods, particles are considered to be point and the effect of presence of particle to the field variables is ignored. In this case, only effect of field variables on the particle is taken into account. Having obtained the field variables without the presence of the particles, particle trajectories can then be evaluated as a result of the post-processing step using correlations to account for the forces on the particles. Therefore, it is possible to simulate multiparticle simulation with a statistical approach using LTM. Due to its ease of implementation and computational efficiency point-particle approach becomes advantageous in cases where relative size of the particles are small compared to the dimensions of the channel, and where (p-p) interaction is negligible [20]. Despite its limitations, LTM has been used extensively for the simulation of particle tracking to avoid the design process in electrokinetic [36, 37] acoustophoretic [38–40] applications.

Finite sized particle approach also known as *stress-tensor* approach, on the other hand, includes finite-size of the particles. In this approach, the field variables are solved together with the presence of finite-sized particles. The resultant force on the particles are obtained by integrating the related stress tensor on the particles' surface. Boundary Element Method (BEM) is a suitable numerical method to simulate particle trajectories in microchannels since modelling of electric, acoustic and/or magnetic field are governed by linear differential equations. BEM posseses advantages compared to other numerical methods such as finite volume method, finite element method (FEM) in terms of its improved accuracy of the solution since BEM is a semi-analytical method (the integral equation is obtained using exact solution of the corresponding problem and numerical approach is involved in the evaluation of the integrals), discretization and modeling of only the boundary of the solution domain and no successive remeshing is needed, possible applications in domains that extend to infinity in either one or

multi dimensions. Regarding manipulation of colloidals, to asses the effect on the particle presence of the field variables requires a remeshing of the domain for the finite volume or element methods. Determination of the the forces acting on the particles requires calculation of the gradient of the field variables. In order to be able to accurately represent gradient of field variables, a fine mesh is required on the particle surface. This becomes troublesome as particle nears a boundary. Thus, it is of utmost importance to employ a numerical model taking into acount of p-w interaction without having to deal with problems stated above [41]. Owing to the aforementioned benefits, BEM has been a useful numerical tool to study hydrodynamics of colloidal suspensions. Briefly, in BEM the particle surface is discretized into elements and both geometry and field variables are approximated using discontinous interpolation functions. The mathematical formulations employed in BEM either lead to Fredholm's interal equations of first kind (FIE-1) and Fredholm's equations of second kind (FIE-2). Quickly summarizing, the formulation of the BEM using FIE-1 is easier as it directly involves physical variables such as the velocities and tractions on the boundaries. However, this introduces a complexity; the resulting system of equations yield ill-conditioned matrices, which requires use of a direct matrix solver. On the other hand, FIE-2 results in a set of well-conditioned integral equations. Therefore, it enables use of iterative solvers for this case. However, the major disadvantage is that FIE2 does not involve phyical variables but rather the density distributions [42]. In this work, direct boundary element method (FIE-1 kind) is employed. The resulting system of equations are *ill-conditioned*. Therefore, these system of equations are solved using a built-in direct MATLAB® solver called *pseudo inverse*(pinv) function.

In this thesis, a boundary element formulation is presented to investigate the p-p and p-w interactions for colloidal cylinder(s) under the action of DC electric field and gravity in the thin EDL limit. The contribution of colloidal forces and DEP are also incorporated in the model by introducing the resulting forces as external forces acting on the particle(s). Colloidal forces are implemented with the prescribed expressions from the literature derived for cylinders, and the DEP force is obtained by integrating the corresponding Maxwell stress tensor (MST) over the particles surfaces. The EK behavior of colloidals in the vicinity of both

conducting and non-conducting wall was investigated. Throughout the simulations, an external electrical field of E_∞, is applied in either x− or y− direction, depending on the type of the planar boundary (i.e. wall or an electrode). The particles' EK motion is governed by the interactions between particles and local electric and flow fields. The electrophoretic motion of particles under externally applied electric field in an unbounded flow could be calculated thanks to Smoluchowski formula. Yet, the presence of wall/other particles introduce complexity to the electrical and hydrodynamic field in the vicinity of the particles, which cannot be predicted with an analytical formula for multi-particle cases. To be able to include these interactions in the model, the flow and electric fields are calculated together with the presence of the particles in the domain. The velocities of the particles in the vicinity of the boundaries are in the order of μm/s. As a result, viscous effects dominate the inertial ones such that $\mathrm{Re} \ll 1$, which is known to be creeping-flow (*i.e.* Stokes) and the flow field is governed by the following PDEs:

$$\nabla \cdot \mathbf{u} = 0 \tag{1.7a}$$

$$0 = -\nabla P + \mu \nabla^2 \mathbf{u} \tag{1.7b}$$

where $\mathbf{u}$ is the velocity field, P is the pressure field, μ is the viscosity of the fluid. The characteristic time scale for the adjustment of the flow field is neglectible compared to the rate at which flow domain changes [43]. Thus, in this study, a quasi-steady approach is taken and steady Stoke's partial differential equations are solved in this analysis. The electric potential field can be obtained by solving the Laplace equation as:

$$\nabla^2 \phi = 0 \tag{1.8}$$

For relatively weak electric fields (< 0.6 V/cm), a Neumann boundary condition is implemented on the electrode as suggested by [27] to simulate EK based aggregation of colloidals [33, 34]. Due to the presence of EDL in the vicinity of each particle, boundaries of the particles are modeled to be insulated boundaries. Since, electric field is weak in magnitude (< 0.6 V/cm) and $1 \ll \kappa/d$ where d is the diameter of the particle and κ is the *Debye-Hückel parameter*, double-layer assumption is made and slip-velocity boundary conditions on both channel and

particle surfaces are implemented:

$$\mathbf{u}_{\mathrm{w}}^{\mathrm{S}} = -\mu_{\mathrm{w}}(\mathbf{I} - \mathbf{nn}) \cdot \nabla\phi \tag{1.9a}$$

$$\mathbf{u}_{\mathrm{p}}^{\mathrm{S}} = -\mu_{\mathrm{p}}(\mathbf{I} - \mathbf{nn}) \cdot \nabla\phi \tag{1.9b}$$

where ($\mu_{\mathrm{w}} = -\varepsilon\zeta_{\mathrm{w}}/\mu$) is the electroosmotic mobility and ($\mu_{\mathrm{p}} = -\varepsilon\zeta_{\mathrm{p}}/\mu$) is the electrophoretic mobility of the particle. Having computed the flow and electric field, the hydrodynamic drag and EK force is calculated by integration of corresponding hydrodynamic and Maxwell Stress Tensors (neglecting magnetic effects):

$$\mathbf{F}^{\mathrm{H}} = \oint_{\partial\mathcal{D}} \left(\mathbf{n} \cdot \boldsymbol{\sigma}^{\mathrm{H}}\right) \mathrm{dl}, \qquad \mathbf{F}^{\mathrm{EK}} = \oint_{\partial\mathcal{D}} \left(\mathbf{n} \cdot \boldsymbol{\sigma}^{\mathrm{MST}}\right) \mathrm{dl}, \tag{1.10a}$$

$$\mathbf{T}^{\mathrm{H}} = \oint_{\partial\mathcal{D}} (\mathbf{x} - \mathbf{x_p}) \times \left(\mathbf{n} \cdot \boldsymbol{\sigma}^{\mathrm{H}}\right) \mathrm{dl}, \qquad \mathbf{T}^{\mathrm{EK}} = \oint_{\partial\mathcal{D}} (\mathbf{x} - \mathbf{x_p}) \times \left(\mathbf{n} \cdot \boldsymbol{\sigma}^{\mathrm{MST}}\right) \mathrm{dl}, \tag{1.10b}$$

where $\mathbf{n}$ is unit vector normal to the surface. $\boldsymbol{\sigma}^{\mathrm{H}}$ and $\boldsymbol{\sigma}^{\mathrm{MST}}$ are defined as:

$$\boldsymbol{\sigma}^{\mathrm{H}} = -p\mathbf{U} + \mu\left[\nabla\mathbf{u} + (\nabla\mathbf{u})^T\right], \qquad \boldsymbol{\sigma}^{\mathrm{MST}} = \varepsilon\left(\mathbf{E} \otimes \mathbf{E} - \frac{1}{2}\mathbf{E}^2\mathbf{U}\right), \tag{1.11}$$

where $\mathbf{U}$ is the unit tensor and symbol $\bigotimes$ denotes the dyadic product. When the distance between the particles and/or wall is in the order of *nanometers*, the colloidal forces (EDL and vdW forces) need to be incorporated. Colloidal forces are computed based on their corresponding potential values based on approximation proposed by Derjaguin's approximation was derived by Ohshima and Hyono [44] as:

$$\Psi^{\mathrm{EDL}}(d) = -\sqrt{8\pi\varepsilon^2\kappa\frac{a_1 a_2}{a_1 + a_2}}\left[\left(\frac{\zeta_1 + \zeta_2}{2}\right)^2 \mathrm{Li}_{1/2}(-e^{-\kappa d}) + \left(\frac{\zeta_1 - \zeta_2}{2}\right)^2 \mathrm{Li}_{1/2}(e^{-\kappa d})\right] \tag{1.12}$$

where d is the distance along the center of gravities between two cylinder surfaces, ζ_i are the zeta potentials of the bodies, κ is the Debye-Hückel parameter, and ϵ is the permittivity of the medium. Inverse of Debye-Hückel parameter, $(1/\kappa)$, represents the characteristic EDL thickness. For an electrolyte with symmetric ions, κ can be written as:

$$\kappa = \sqrt{\frac{2z^2e^2n_\infty^2}{\varepsilon k_B T}} \tag{1.13}$$

where z is the valence of the ions, e is the elementary charge, n_∞ is the bulk ionic concentration, k_B is Boltzmann's constant, and T is the absolute temperature.

In Eq. 1.12, Li is defined as polylogarithmic function:

$$\mathrm{Li_s(z)} = \sum_{\mathrm{k=1}}^{\infty} \frac{\mathrm{z^k}}{\mathrm{k^s}} \tag{1.14}$$

The EDL force between two cylinders along the line connecting the centers can be determined by differentiating EDL interaction energy with respect to distance between particles' surfaces:

$$\mathbf{f}^{\mathrm{EDL}} = -\frac{\partial \Psi^{\mathrm{EDL}}}{\partial \mathrm{d}} \tag{1.15}$$

The vdW interaction potential between two cylinders is defined as:

$$\Psi^{\mathrm{vdW}}(d) = \frac{A_{132}}{12\sqrt{2}d^{3/2}} \left(\frac{a_1 a_2}{a_1 + a_2} \right)^{1/2} \tag{1.16}$$

where A_{132} is the Hamaker constant for the materials 1 and 2 in the presence of the medium 3, $\mathrm{a_i}$ are the radii of the particles, d is the distance between the surfaces' of the cylinders. Similarly, the vdW force along the line connecting particles' centers can be obtained by differentiating corresponding interaction potential as:

$$\mathbf{f}^{\mathrm{vdW}} = -\frac{\partial \Psi^{\mathrm{vdW}}}{\partial d} = -\frac{A_{132}}{8\sqrt{2}d^{5/2}} \left(\frac{a_1 a_2}{a_1 + a_2} \right)^{1/2} \tag{1.17}$$

In this work, in order to capture the physics of the problem accurately, the value for Hamaker constant, $A_{132} = (3/4\pi)\hbar\bar{\omega}_{132}$ is selected for polystrene (PS) and gold (Au) pairs in deionized water in the form of Lifshitz -van der Waals Constant, $\hbar\bar{\omega}_{132}$= 0.72 eV for PS-Au and 0.11 eV for PS-PS interactions [45]. Following Eqs. (1.15) and (1.17), the colloidal forces between the particle and a wall could be determined by taking the limit when the radius of one cylinder goes to infinity. One has to note that Eqs. (1.12) and (1.16) incorporate only pairwise interactions. At the end, to model a three body interaction (p-p and p-w), a superposition of p-p and p-w interactions are implemented. In table 1.1, a summary of the literature is presented. Numerous works are grouped under separate categories based on boundary condition choices, dimensionality of the problem and included forces.

Table 1.1: Summary of the Literature

Author	Year	Particle		Wall		Electric Field Direction					Forces		Electric Field	
		Sphere	Cylinder	Cond. Wall	Non-Cond. Wall	Parallel	Perpendicular		p-p	p-w	DEP	Colloidal	DC	AC
							Dirichlet	Neuman						
Keh *et al.* [46]	1985				✓	✓	✓			✓			✓	
Keh *et al.* [25]	1988	✓			✓	✓				✓			✓	
Keh *et al.* [30]	1991		✓	✓	✓	✓	✓			✓			✓	
Solomentsev *et al.* [35]	2000	✓		✓			✓						✓	
Yariv *et al.* [26]	2003	✓			✓	✓				✓			✓	
Fagan *et al.* [33]	2004	✓		✓			✓			✓				✓
Young Li *et al.* [15]	2005	✓			✓	✓				✓	✓	✓	✓	
Fagan *et al.* [34]	2006	✓		✓			✓		✓	✓				✓
Ristenpart *et al.* [27]	2007	✓		✓				✓		✓			✓	
Ristenpart *et al.* [28]	2007	✓		✓				✓		✓				✓
Saintillian *et al.* [47]	2008	✓							✓		✓		✓	
LaMagna *et al.* [48]	2009	✓							✓		✓		✓	
Yariv *et al.* [29]	2010	✓		✓				✓		✓			✓	
Wang Keh *et al.* [31]	2011		✓	✓	✓	✓	✓			✓			✓	
House *et al.* [49]	2011	✓			✓					✓			✓	
House *et al.* [50]	2012								✓		✓		✓	
Dutta *et al.* [23]	2013		✓				✓		✓		✓		✓	
Dutta *et al.* [51]	2014		✓	✓			✓		✓		✓		✓	✓
LaMagna *et al.* [17]	2015	✓		✓	✓					✓	✓			✓
S. Kang *et al.* [52]	2015		✓						✓					✓
Yariv *et al.* [18]	2016	✓			✓	✓				✓	✓		✓	
Yariv *et al.* [19]	2016		✓	✓	✓	✓		✓		✓			✓	
Cetin *et al.* [20]	2017		✓	✓	✓	✓	✓		✓	✓	✓			
S. Kang *et al.* [24]	2017		✓		✓	✓				✓	✓			
Present Study	2021		✓	✓	✓	✓	✓	✓	✓	✓	✓	✓	✓	

1.2 Objectives and Motivation

There is no rigorous model resolving p-p and p-w interactions of colloidals with the inclusion of DEP and colloidal forces in the vicinity of a planar boundary. In this work, the results obtained from a set of boundary element simulations regarding electrokinetic behavior of colloidal(s) in the vicinity of a planar boundary are presented. In the literature, there are a number of theoretical and numerical studies analyzing p-p [20–24, 32] and p-w [15–20, 25–31, 33–35, 53] interactions. However, to the best of author's knowledge, this is the first study in which electrokinetic behavior of colloidals in close proximity to a planar wall is simulated with a detailed examination of particle-particle and particle-wall interactions together with the inclusion of colloidal and dielectrophoretic (DEP) forces. Initially, once the particle approached to an external boundary, oscillations on the particle velocities were observed. In order to overcome numerical oscillations, geometry and the field variables were approximated using quadratic polynomials. Also, time scheme for the simulations were upgraded from explicit Euler to second order explicit Adams-Bashforth method. In order to decrease computational cost of the code, an adaptive mesh algorithm was used. In addition, the code is parallelized using a built-in MATLAB® *parfor* function from parallel toolbox. As a result of this work, an accurate, adaptive inhouse boundary element method solver simulating behavior of colloidal interactions in the vicinity of a planar boundary has been developed.

1.3 Thesis Outline

In this section, a brief summary of each chapter is included. **Chapter 1:** A brief introduction to microfluidics theory is made. Exemplary applications to the EK manipulation of colloidals are given. Definitions to fundamental electrokinetic concepts such as *electroosmosis, electrophoresis, dielectrophoresis* are made. In addition, a detailed literature review on colloidal dynamics is listed. At the end of the first chapter, the objective, motivation and outline of the thesis is presented.

Chapter 2: A detailed mathematical background of the boundary element formulation for the flow (governed by Stoke's equation) and potential field (governed by Laplace equation) is given. Then, detailed information regarding particle tracking formulation is shared. Finally, the flowchart regarding the algorithm of the custom solver is given. **Chapter 3:** In this chapter, verification of the multiphysics simulations are presented. As for hydrodynamic benchmarks, drag forces acting on a particle for the case of next to a single wall and two walls are computed and compared with their respective analytical solutions. In hydrodynamic simulations, the pressure distribution in a channel with an obstacle in the middle is compared with the analytical solution for the same problem given by *Faxèn et al.* [54]. Concerning electrokinetic benchmarks, the EK particle velocities of the particles under various settings including a conducting and a non-conducting wall are computed and compared with respective analytical solutions given by *Keh et al.* [30, 31]. Finally, the electric field computed by BEM is compared with the analytical solution for a 2-D Laplace problem involving dirichlet boundary conditions. **Chapter 4:** DC electrokinetic behavior of particle(s) is simulated in the vicinity of both a conducting and a non-conducting wall. For the particles next to a conducting wall (ie. anode), the effect of boundary condition to the particle behavior is analyzed. Throughout the simulations, Dirichlet and Neuman boundary conditions are implemented. As a result of the simulations, it was shown that Neumann boundary condition introduces *electrohydrodynamic flow (EHD)* phenomenon, which gravely affects lateral colloidal aggregation under DC electric field. In the second part of the thesis, DC electrokinetic behavior of colloidals next to a non-conducting wall is investigated and particle-particle interactions are analyzed in detail. Finally, outcomes are reported and a general discussion is made. **Chapter 5:** Concluding marks are made and the future directions of the current research is discussed.

Chapter 2

Boundary Element Formulation

In this section, detailed information regarding the Boundary Element Method formulation for fluid flow and electrical field is presented. In addition, custom formulation regarding particle tracking is elucidated. Lastly, a flowchart describing the algorithm of the custom solver is presented.

2.1 Fluid Flow Model

For a point lying on the boundary ∂D, the boundary integral representation of 2D Stokes equations become [55]:

$$\frac{1}{2}\mathbf{u}(\mathbf{x_o}) = -\frac{1}{4\pi\mu}\int_{\partial\mathcal{D}} \mathbf{t}(\mathbf{x})\boldsymbol{\mathcal{G}}^{\mathrm{S}}(\mathbf{x_o},\mathbf{x})\mathrm{dl}(\mathbf{x}) + \frac{1}{4\pi}\int_{\partial\mathcal{D}} \mathbf{u}(\mathbf{x})\Big[\nabla\boldsymbol{\mathcal{G}}^{\mathrm{S}}(\mathbf{x_o},\mathbf{x})\cdot\mathbf{n}(\mathbf{x})\Big]\mathrm{dl}(\mathbf{x}) \quad (2.1)$$

where $\mathbf{t} \equiv \boldsymbol{\sigma}\cdot\mathbf{n}$ is the traction vector, and $\boldsymbol{\mathcal{G}}^{\mathrm{S}}(\mathbf{x_o},\mathbf{x})$ is the free-space Green's function for 2D Stokes equation (*i.e.* Stokeslet):

$$\boldsymbol{\mathcal{G}}^{\mathrm{S}}(\mathbf{x_o},\mathbf{x}) = \frac{1}{4\pi\mu}\Big[-\mathbf{I}\ln|\mathbf{r}| + \frac{\mathbf{r}\otimes\mathbf{r}}{|\mathbf{r}|^2}\Big] \quad (2.2)$$

where $\mathbf{r} = \mathbf{x} - \mathbf{x_o}$ and $\nabla\boldsymbol{\mathcal{G}}^{\mathrm{S}}(\mathbf{x_o},\mathbf{x})$ is the stress tensor of the free-space Green's function for the Stoke's problem (*i.e.* stresslet), respectively. The integral equations for the velocity can be discretized and the boundary integrals can be approximated as the sums of integrals across surface elements $\mathrm{E_n}$ ($\mathrm{n} = 1, 2\cdots\mathrm{N}$).

Employing quadratic functions for the field variables across the elements, discretized integrals for Laplace and Stokes equations become:

$$\mathrm{H}^{\mathrm{S}^{(\mathrm{n})}}(\mathbf{x_o}) = \int_{\mathrm{E_n}} \left(\sum_{\mathrm{m}=1}^{\mathrm{M}} \psi_{\mathrm{m}} \mathbf{u}_{\mathrm{m}}^{\mathrm{n}}(\mathbf{x}) \right) \left[\nabla \boldsymbol{\mathcal{G}}^{\mathrm{S}}(\mathbf{x_o}, \mathbf{x}) \cdot \mathbf{n}(\mathbf{x}) \right] \mathrm{dl}(\mathbf{x}) \tag{2.3a}$$

$$\mathrm{G}^{\mathrm{S}^{(\mathrm{n})}}(\mathbf{x_o}) = \int_{\mathrm{E_n}} \left(\sum_{\mathrm{m}=1}^{\mathrm{M}} \psi_{\mathrm{m}} \mathbf{t}_{\mathrm{m}}^{\mathrm{n}}(\mathbf{x}) \right) \boldsymbol{\mathcal{G}}^{\mathrm{S}}(\mathbf{x_o}, \mathbf{x}) \mathrm{dl}(\mathbf{x}) \tag{2.3b}$$

where ψ_{m}, $(q')_{\mathrm{m}}^{\mathrm{n}} = [\mathbf{n} \cdot \nabla(\phi')(\mathbf{x})_{\mathrm{m}}^{\mathrm{n}}]$, and $(\phi')_{\mathrm{m}}^{\mathrm{n}}$ are the shape functions of each node, the values of normal flux, and the potential values of the mth nodes of nth element residing on the boundaries at each element, respectively. For a load point on a single element, the discretized boundary integral equations can be written as:

$$\frac{1}{2}\mathbf{u}(\mathbf{x_o}) + \frac{1}{4\pi\mu} \sum_{\mathrm{n}=1}^{\mathrm{N}} \mathrm{H}^{\mathrm{S}^{(\mathrm{n})}}(\mathbf{x_o}) = \frac{1}{4\pi} \sum_{\mathrm{n}=1}^{\mathrm{N}} \mathrm{G}^{\mathrm{S}^{(\mathrm{n})}}(\mathbf{x_o}) \tag{2.4}$$

The main goal is to determine the unknown field variables on the boundaries. Among the weighted residual methods, due to its versatility and computational efficiency, the collocation method is implemented to transform the boundary integral equations into sets of linear equations leading to two matricess named as G^{S}, and H^{S} for Stokes problems [56]. If diagonals are augmented with 1/2, the augmented matricess can be recast into:

$$\widetilde{\mathbf{H}}^{\mathrm{S}}(\mathbf{x_o}, \mathbf{x}) \cdot \{\mathbf{u}\} = \widetilde{\mathbf{G}}^{\mathrm{S}}(\mathbf{x_o}, \mathbf{x}) \cdot \{\mathbf{t}\} \tag{2.5}$$

where $\{\phi'\}$ is the vector containing the potential values of the nodes on the boundary elements and $\{q'\}$ is the corresponding vector for the normal fluxes. Since BEM is a mixed formulation, as it is seen in equation 2.5, depending on the boundary conditions, either the electric potentials or the normal fluxes on the elements are known [56]. Known boundary conditions are collected at appropriate side with a column switch. Either the velocity or the traction values are known on the wall. However, neither velocity nor traction values are known on the particle surface. Following the appropriate column switching, a linear system of equations can be obtained for the unknown quantities located on the nodes of the boundary elements. Once velocity and traction values are determined for all surface elements, the pressure and velocities in the domain can be calculated at

a later step as a post-processing.

$$\mathrm{P}(\mathbf{x_o}) = \int_{\mathcal{D}} \mathbf{t}(\mathbf{x})\mathbf{p}(\mathbf{x_o},\mathbf{x})\mathrm{dl}(\mathbf{x}) - \mu \int_{\mathcal{D}} \mathbf{\Pi}(\mathbf{x_o},\mathbf{x})\ \mathbf{u}(\mathbf{x})\mathrm{dl}(\mathbf{x}) \tag{2.6}$$

where $\mathbf{p}$ is the pressure Green's function and $\mathbf{\Pi}$ is stress tensor associated with stresslet [55]. As for the velocity values in the domain, equation 2.1 could be used. However, the velocity at a certain point within the domain is obtained by the evaluation of Eq. (2.1) with the coefficient of unity in front of the $\mathbf{u}(\mathbf{x}_o)$ term instead of 1/2.

2.2 Electrical Field Model

To utilize the free-space Green's function in the solution, the electric potential field is decomposed into two component. These consist of background potential and disturbance potential:

$$\phi(\mathbf{x}) = \phi'(\mathbf{x}) + \phi_\infty \tag{2.7}$$

where ϕ^∞ is the background electric potential that results in a constant E_∞ in either x or y–direction, and ϕ' is the disturbed electric potential. Referring to figure 4.4, background potential is linked to background electric field by $\boldsymbol{\phi}_\infty = -\mathrm{E}_\infty \cdot \mathbf{y}$. Note that such a decomposition makes the non-homogeneous boundary condition on the electrode a homogeneous one, and vice versa for the boundary condition on the particle surface. For a point lying on the boundary ∂D, the boundary integral representation of 2D Laplace and Stokes equations are of the following form [55]:

$$\begin{aligned}\frac{1}{2}\phi'\left(\mathbf{x_o}\right) = &-\int_{\partial\mathcal{D}} \mathcal{G}^{\mathrm{L}}\left(\mathbf{x_o},\mathbf{x}\right)\Big[\mathbf{n}(\mathbf{x})\cdot\nabla\phi'(\mathbf{x})\Big]\mathrm{dl}(\mathbf{x}) \\ &+\int_{\partial\mathcal{D}} \phi'(\mathbf{x})\Big[\mathbf{n}(\mathbf{x})\cdot\nabla\mathcal{G}^{\mathrm{L}}(\mathbf{x_o},\mathbf{x})\Big]\mathrm{dl}(\mathbf{x})\end{aligned} \tag{2.8}$$

where $\mathcal{G}^{\mathrm{L}}(\mathbf{x_o},\mathbf{x})$ is the free-space Green's function for 2D Laplace equation.

$$\mathcal{G}^{\mathrm{L}}(\mathbf{x_o},\mathbf{x}) = -\frac{1}{2\pi}\ln|\mathbf{r}| \tag{2.9}$$

where $\mathbf{r} = \mathbf{x} - \mathbf{x_o}$ and $\nabla\mathcal{G}^{\mathrm{L}}(\mathbf{x_o}, \mathbf{x})$ is the gradient of the Green's fundamental solution for the Laplace problem. The integral equations for the potential and flux values can be discretized and the boundary integrals can be approximated as the sums of integrals across surface elements $\mathrm{E_n}$ ($\mathrm{n} = 1, 2 \cdots \mathrm{N}$). Employing quadratic functions for the field variables across the elements, discretized integrals for Laplace equation become:

$$\mathrm{H}^{\mathrm{L}^{(\mathrm{n})}}(\mathbf{x_o}) = \int_{\mathrm{E_n}} \left(\sum_{\mathrm{m}=1}^{\mathrm{M}} \psi_{\mathrm{m}} (\phi')^{\mathrm{n}}_{\mathrm{m}}(\mathbf{x}) \right) \left[\mathbf{n}(\mathbf{x}) \cdot \nabla\mathcal{G}^{\mathrm{L}}(\mathbf{x_o}, \mathbf{x}) \right] \mathrm{dl}(\mathbf{x}) \tag{2.10a}$$

$$\mathrm{G}^{\mathrm{L}^{(\mathrm{n})}}(\mathbf{x_o}) = \int_{\mathrm{E_n}} \left(\sum_{\mathrm{m}=1}^{\mathrm{M}} \psi_{\mathrm{m}} (q')^{\mathrm{n}}_{\mathrm{m}}(\mathbf{x}) \right) \mathcal{G}^{\mathrm{L}}(\mathbf{x_o}, \mathbf{x}) \mathrm{dl}(\mathbf{x}) \tag{2.10b}$$

where ψ_{m}, $(q')^{\mathrm{n}}_{\mathrm{m}} = [\mathbf{n} \cdot \nabla(\phi')(\mathbf{x})^{\mathrm{n}}_{\mathrm{m}}]$, and $(\phi')^{\mathrm{n}}_{\mathrm{m}}$ are the shape functions of each node, the values of normal flux, and the potential values of the mth node of n^{th}element residing at each element residing on the boundary, respectively. For a load point on a single element, the discretized boundary integral equations can be written as:

$$\frac{1}{2}\phi'(\mathbf{x_o}) + \sum_{n=1}^{N} \mathrm{H}^{\mathrm{L}^{(\mathrm{n})}}(\mathbf{x_o}) = \sum_{\mathrm{n}=1}^{\mathrm{N}} \mathrm{G}^{\mathrm{L}^{(n)}}(\mathbf{x_o}) \tag{2.11}$$

Similiar to Stoke's equations, the main goal is to determine the unknown field variables on the boundaries once again. Among the weighted residual methods, due to its versatility and computational efficiency, the collocation method is implemented to transform the boundary integral equations into sets of linear equations leading to two matricess named as $\mathrm{G^L}$ and $\mathrm{H^L}$ for Laplace problems [56]. If diagonals are augmented with 1/2, the augmented matricess can be transformed into:

$$\widetilde{\mathbf{H}}^{\mathrm{L}}(\mathbf{x_o}, \mathbf{x}) \cdot \{\boldsymbol{\phi}'\} = \widetilde{\mathbf{G}}^{\mathrm{L}}(\mathbf{x_o}, \mathbf{x}) \cdot \{\mathbf{q}'\} \tag{2.12}$$

where $\{\boldsymbol{\phi}'\}$ is the vector containing the potential values of the nodes on the boundary elements and $\{\mathbf{q}'\}$ is the corresponding vector for the normal fluxes. Depending on the boundary conditions, either the electric potentials or the normal fluxes on the elements are known. Following the appropriate column switching, a linear system of equations can be obtained for the unknown quantities on the nodes of the boundary elements. Once the electric potential values are determined for all surface elements, the tangential electric field values on each element can be

calculated *via* the derivatives of the fundamendal solutions. Having the normal and tangential electric field values on the boundaries, slip-velocities on the wall and the particles' surfaces can be evaluated. Moreover, EK force and torque values for each particle can also be determined by integrating the MSTs over the particles' surfaces. In the post-processing step, the electric field is computed by the following expression [56].

$$\frac{\partial \phi'}{\partial \mathbf{x_o}} = \int_{\partial \mathcal{D}} \left(q' \frac{\partial \mathcal{G}^{\mathrm{L}}}{\partial \mathbf{x}} \bigg|_{\mathbf{x_o}} - \phi' \frac{\partial \left(\nabla \mathcal{G}^{\mathbf{L}} \right)}{\partial \mathbf{x}} \bigg|_{\mathbf{x_o}} \right) \mathrm{dl}(\mathbf{x}) \tag{2.13}$$

Potential values in the domain are computed from the equation 2.8. Similiar to the computation of velocity values in the domain, coefficient of potentials should be unity instead of 1/2.

2.3 Particle Tracking

Particle tracking is implemented using a technique through which a partitioning process was used to speed up the calculations, detailed in formation regarding partition procedure could be found in Cetin et al [57]. As stated in their formulation, the constraints associated with rigid body motion can be imposed for the closure of the problem as:

$$\mathbf{u}_{\mathrm{p}} = \mathbf{u}^{\mathrm{B}} + \omega^{\mathrm{B}} \times \mathbf{r}_{\mathrm{p}} + \mathbf{u}_{\mathrm{p}}^{\mathrm{S}} \tag{2.14}$$

where $\mathbf{u}_{\mathrm{p}}$ is the velocity at a node on the boundary of the particle, $\mathbf{u}^{\mathrm{B}}$ is the velocity of the selected center of the particle, ω^{B} is the angular velocity and $\mathbf{r}_p$ is the relative position vector of the boundary node to the center of the particle and $\mathbf{u}_{\mathrm{p}}^{\mathrm{S}}$ is the slip-velocity on the particle surface given in Eq. (1.9b). Imposing Eqn. (2.14), all the boundary points on the particle can be related to the linear and angular velocities at the centroid of the particles through a kinematic matrix $\mathbf{M}$ as:

$$\begin{aligned} \mathbf{u}_{\mathrm{p}} &= \mathbf{M} \cdot \mathbf{u}^{\mathrm{B}} + \mathbf{u}_{\mathrm{p}}^{\mathrm{S}} \\ \mathbf{u}^{\mathrm{B}} &= \left\{ \begin{array}{cccccc} u_{\mathrm{x},1}^{\mathrm{B}} & u_{\mathrm{y},1}^{\mathrm{B}} & \omega_1^{\mathrm{B}} & u_{\mathrm{x},2}^{\mathrm{B}} & u_{\mathrm{y},2}^{\mathrm{B}} & \omega_2^{\mathrm{B}} \end{array} \right\}^{\mathbf{T}} \end{aligned} \tag{2.15}$$

where $\mathbf{u}_{\mathrm{B}}$ contains the linear and angular velocities at the center of gravity of each particle. Similarly, the force and moment on each particle can be obtained in a matrix form as [58]:

$$\begin{aligned} \mathbf{f}^{\mathrm{B}} &= \mathbf{F} \cdot \mathbf{t}_{\mathrm{p}} \\ \mathbf{f}^{\mathrm{B}} &= \left\{ \begin{array}{cccccc} \mathrm{f}^{\mathrm{B}}_{\mathrm{x},1} & \mathrm{f}^{\mathrm{B}}_{\mathrm{y},1} & \mathrm{M}^{\mathrm{B}}_{1} & \mathrm{f}^{\mathrm{B}}_{\mathrm{x},2} & \mathrm{f}^{\mathrm{B}}_{\mathrm{y},2} & \mathrm{M}^{\mathrm{B}}_{2} \end{array} \right\}^{\mathbf{T}} \end{aligned} \tag{2.16}$$

where $\mathbf{f}_B$ contains the net force and moments with respect to center of gravity of each particle. Following the formulation from our previous study [Eq. (22) in [58]], the relation between the force acting on the particles and the rigid body velocity of the particles can be written as:

$$\mathbf{f}^{\mathrm{B}} = \mathbf{K} \cdot \mathbf{u}^{\mathrm{B}} + \mathbf{L} \cdot \mathbf{u}^{\mathrm{S}}_{\mathrm{p}} + \mathbf{b} = \mathbf{f}_{\mathrm{ext}} \tag{2.17}$$

where $\mathbf{b}$ has the contribution of the slip-velocity on the wall given in Eq. (1.9a) and $\mathbf{f}_{\mathrm{ext}}$ is the external force acting on the particle apart from the hydrodynamic drag. In our study, there are four components for the external force: (i) gravity, (ii) DEP force (obtained with the integration of MST over the particles' surfaces), (iii) the force corresponds to the EDL and (iv) vdW interactions associated with the pairwise particle-particle and particle-wall interactions. The rigid body velocities of the particles can be determined using Eq. (2.17), and thanks to the linearity of the problem, the rigid-body velocity can be decomposed into velocities associated with the different external force components as:

$$\mathbf{u}^{\mathrm{B}} = \mathbf{u}^{\mathrm{S}}_{\mathrm{w}} + \mathbf{u}^{\mathrm{G}} + \mathbf{u}^{\mathrm{EK}} + \mathbf{u}^{\mathrm{C}} \tag{2.18}$$

where

$$\begin{aligned} \mathbf{u}^{\mathrm{S}}_{\mathrm{w}} &= -\mathbf{K}^{-1} \cdot \mathbf{b}, \quad & \mathbf{u}^{\mathrm{EK}} &= \mathbf{K}^{-1} \cdot (\mathbf{f}^{\,\mathrm{DEP}}_{\mathrm{ext}} - \mathbf{L} \cdot \mathbf{u}^{\mathrm{S}}_{\mathrm{p}}) \\ \mathbf{u}^{\mathrm{G}} &= \mathbf{K}^{-1} \cdot \mathbf{f}^{\mathrm{G}}_{\mathrm{ext}}, \quad & \mathbf{u}^{\mathrm{C}} &= \mathbf{K}^{-1} \cdot (\mathbf{f}^{\,\mathrm{EDL}}_{\mathrm{ext}} + \mathbf{f}^{\,\mathrm{vdW}}_{\mathrm{ext}}) \end{aligned} \tag{2.19}$$

$\mathbf{u}^{\mathrm{S}}_{\mathrm{W}}$ is the contribution of the slip-velocity on the wall, $\mathbf{u}^{\mathrm{G}}$ is the contribution of the gravity (*i.e.* sedimentation velocity), $\mathbf{u}^{\mathrm{EK}}$ is the contribution of the DEP and slip-velocity on the particle surface and $\mathbf{u}^{\mathrm{C}}$ is the combined contribution of EDL and vdW (*i.e.* colloidal forces). Once the rigid body velocity of the particle is determined, the trajectory of the particles are obtained by employing a second-order Adam-Bashford time integration scheme:

$$\mathbf{x}^{\mathrm{B}}_{\mathrm{n+1}} = \mathbf{x}^{\mathrm{B}}_{\mathrm{n}} + \mathbf{u}^{\mathrm{B}}(t_{\mathrm{n}}, \mathbf{x}^{\mathrm{B}}_{\mathrm{n}})\Delta t \tag{2.20a}$$

$$\mathbf{x}^{\mathrm{B}}_{\mathrm{n+2}} = \mathbf{x}^{\mathrm{B}}_{\mathrm{n+1}} + \left[3/2\, \mathbf{u}^{\mathrm{B}}(t_{\mathrm{n+1}}, \mathbf{x}^{\mathrm{B}}_{\mathrm{n+1}}) - 1/2\, \mathbf{u}^{\mathrm{B}}(t_{\mathrm{n}}, \mathbf{x}^{\mathrm{B}}_{\mathrm{n}})\right] \Delta t \tag{2.20b}$$

2.4 Algorithm of the Solver

The EK motion of the particles is simulated via a custom solver typed in MATLAB® environment. In order to obtain an efficient code following features are implemented in the code:

- Adaptive mesh algorithm,
- Parallelization of the solver,
- Automatic time step computation,
- One time computation of the H^S_{oo}, H^L_{oo}, ${G_{oo}}^S$, and G^L_{oo} matrices containing information from non-moving mesh (channel).

Initially, necessary basic information such as dimensions of the channel and colloidals, total number of colloidals, material properties, magnitude of the electrical field and so on are input. Having completed the first step, the code creates a vector that contains meshing conditions. Algorithm then scans this vector containing conditions to create a specific mesh at a specific location for the colloidals. With this condition, it is possible to create a course mesh in the beginning and then increase the mesh quality as the colloidals approach at each other. Since particle tracking formulation allows independent matrix factorization, *parfor* function from MATLAB® library is used. Parallel computation of multiphysics matrices shortens the total simulation time. Regarding time step computations, *second-order Adams-Bashforth* time scheme was utilized. To obtain a quadratic time scheme, time step has to be constant in computations. In this case, if the velocity change exceeds a preset value, the algorithm replaces current mesh with the previous mesh from one time step earlier, halves time step and recomputes matrices as it is seen in figure 2.1. Throughout the computations, the time step is halved only once, which resulted in a loss of accuracy for that single time step. Finally, in order to reduce total simulation time, matrices containing information from non-moving mesh is computed only once, which is computed only at the beginning of the computation.

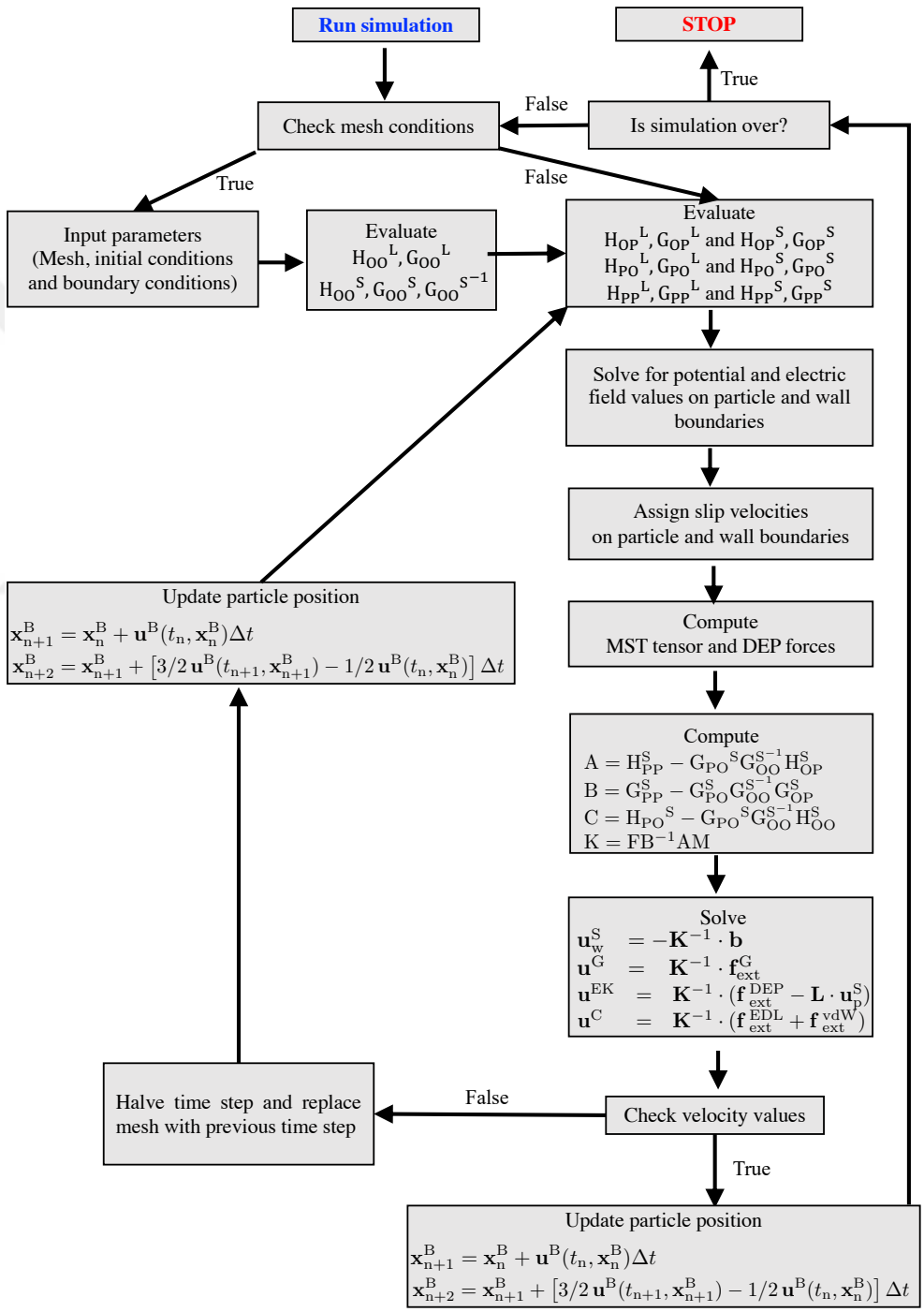

Figure 2.1: Flow chart of the custom algorithm used in present study

Chapter 3

Validation of the Model

Validation of the computational model is carried out via hydrodynamic and electrokinetic benchmarks. Both hydrodynamic and electrokinetic benchmarks consist of three problems under different settings.

For the hydrodynamic benchmark, drag force acting on a particle is computed under two different settings: in the vicinity of a single wall and between a double wall. Numerical results are compared with the analytical ones given by Onishi *et al.* [59] and Richou *et al.* [54] for particle near a single wall and for a particle between two walls, respectively. In order to verify post-process, pressure values computed with BEM are compared with pressure values along the channel obtained by analytical solution proposed by *Faxèn et al.* [54] for the case of an obstacle moving with constant speed between a double wall.

Electrokinetic benchmarks include electrophoretic velocity of the particle in various settings at which the direction of the electric field changes. Electrophoretic velocity of the particle obtained by BEM near a conducting wall (electric field is perpendicular to the wall) and a non-conducting wall (electric field is parallel to the wall) is compared with analytical solutions given by Keh *et al.* [30]. In post processing, the potential and electric field computed by BEM is compared with analytical solution for a 2-D Laplace equation.

3.1 Hydrodynamic Benchmarks

3.1.1 Drag Force on a Particle next to a Single Wall

Concerning flows involving small Re numbers (*ie. creeping flow*), there exists an analytical solution describing the behavior of a colloidal moving past a non-moving wall. he schematical drawing of such problem is given in figure 3.1. For a circular cylindrical particle moving past a single wall, total torque acting on the particle is zero. Similiarly, for a rotating particle next to a wall, the total force acting on it is zero. Such conclusions and the analytical solution to the problem at hand are given by Onishi *et al.* [59]:

$$\lambda = \frac{\mathrm{F_{Drag,analytical}}}{\mu \mathrm{U_p}} = \frac{-4\pi}{\log\{\mathrm{r}^{-1}[\mathrm{y_C} + (\mathrm{y_C^2} - \mathrm{r}^2)^{1/2}]\}} \tag{3.1}$$

where d is the distance between center of gravity of the particle and the wall, r is the radius of the particle and $\mathrm{a}^2 = \mathrm{y_C^2} - \mathrm{r}^2$. As expected, the closer particle moves past the boundary, hydrodynamic drag force acting on the particle increases and as the particle gets away from the wall, the total drag force acting on the particle decreases.

In BEM formulation, he total drag force acting on the particle is directly computed from summation of the traction values of corresponding nodes residing

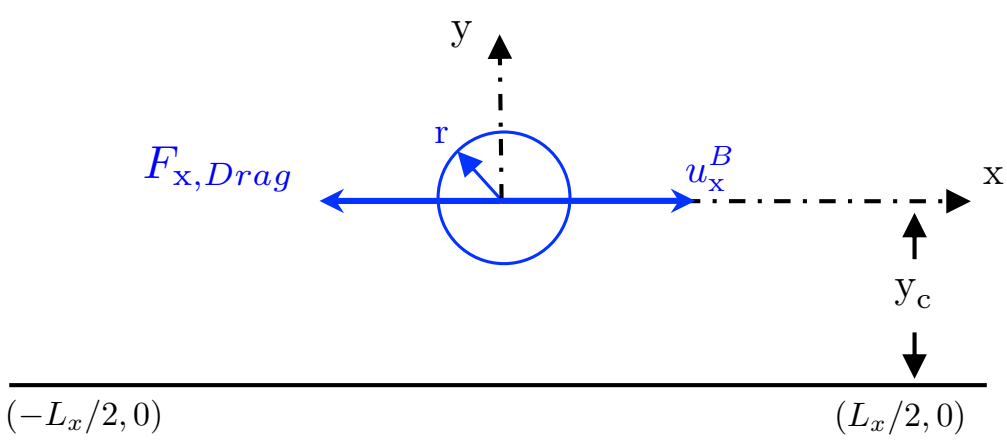

Figure 3.1: Schematics of hydrodynamic benchmark with a single wall

Table 3.1: Comparison of BEM vs analytical solution of drag force acting on a cylindrical object in the vicinity of a single wall

$\mathbf{r/y_C}$	**BEM**	**Onishi *et al.* [59]**	**Error [%]**
5	5.4817	5.4817	0.0013
10	4.1981	4.1983	0.0032
20	3.4070	3.4071	0.0031
30	3.0692	3.0694	0.0062
50	2.7284	2.7288	0.0152
100	2.3705	2.3718	0.0528

on the element:

$$\mathbf{F}_{\mathrm{Drag}}^{\mathrm{BEM}} = \sum_{\mathrm{n}=1}^{\mathrm{E}} \sum_{\mathrm{m}=1}^{3} \int_{\partial\mathcal{D}} \mathbf{t}_{\mathrm{m}}^{\mathrm{n}} \cdot \psi_{\mathrm{m}} \, \mathrm{d}\Gamma \tag{3.2}$$

where $\mathbf{t}_{\mathrm{m}}^{\mathrm{e}}$ is the traction value of mth node located at e^{th} element on the boundary and ψ_{m} is the shape function associated with the related nodal value. Throughout the formulation, quadratic elements was utilized for the discretization of field variables. Thus, firstly nodal traction values were to be multiplied with their associated shape functions. Then the sum of these nodal values for each element had to be summed up. As a result, the drag force acting on a particle was obtained.

In table 3.1, it is apparent that as the particle moves away from the wall the error increases. This is because as the particle gets away from the wall, the length of the wall needs to be increased to obtain an accurate result. This is an outcome of the single wall formulation used throughout the simulations. As the length of the wall increases, even though number of elements are increased, due to computational limitations, number of total elements used on wall is limited. This results in a decrease in accuracy. Throughout the simulations, a mesh of 10μm/element for the wall and 0.5μm/element on particle was implemented.

3.1.2 Drag Force on a Particle Between Two Walls

In conventional fluid mechanics, the presence of the walls introduce viscous forces acting on the particle. For a particle between two walls, as the gap between

walls close, the hydrodynamic force exerted on the particle increases. Two-wall hydrodynamic benchmark is given in figure 3.2.

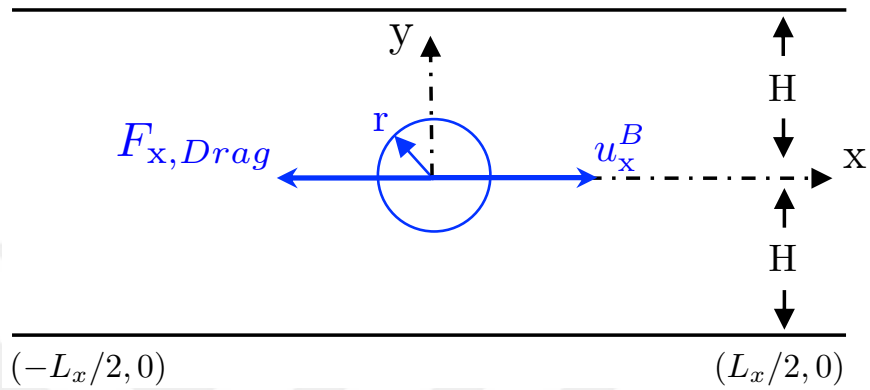

Figure 3.2: Schematics of hydrodynamic benchmark with a double wall

In 2-D, Faxèn *et al.* [54] found an analytical expression for the drag force where a particle with a constant velocity moves between two walls. They reported drag force as a non-dimensional quantity in the following form :

$$\begin{aligned} \lambda(\mathrm{k}) &= \frac{F_x(k)}{\mu \mathrm{U}_0} \\ &= \frac{4\pi}{A_0 - \ln(k) + A_2 k^2 + A_4 k^4 + A_6 k^6 + A_8 k^8} \end{aligned} \tag{3.3}$$

where

$$\begin{aligned} &A_0 = -0.9156892732, \quad A_2 = 1.7243844 \\ &A_4 = -1.730194, \quad A_6 = 2.405644, \\ &A_8 = -4.59131 \quad \text{and} \quad \mathrm{k} = \mathrm{r}/\mathrm{H} \end{aligned} \tag{3.4}$$

Similiar to the single-wall case, hydrodynamic force acting on a particle is calculated using equation 3.2. The comparison of linear BEM, quadratic BEM and the analytical solution could be seen in the table 3.1.2. Throughout the computations, non-uniform mesh both on the channel walls and on the particle was used. The length of the channel walls were set to 50 times the diameter of the particle.

Table 3.2: Comparison between present study, Richou *et al.* [54], and analytical solution given by Faxèn *et al.* [54] for the calculation of hydrodynamic drag force acting on a particle between a double wall.

r/H	**Present Study (PS)**	**Results From [54]**	**Faxèn *et al.* [54]**	**Error [%] (PS)**	**Error [%] [54]**
0.010	3.4079	3.5401	3.4058	0.06	3.90
0.025	4.5322	4.7145	4.5296	0.05	4.10
0.050	6.0310	6.1027	6.0289	0.03	3.20
0.100	8.9401	8.1752	8.9506	0.11	2.80
0.200	16.5045	16.7335	16.5326	0.15	1.20
0.400	52.3033	52.8979	52.5669	0.50	0.60
0.800	1596.3012	1629.8050	-	-	-
0.950	51,521.6698	64,884.4322	-	-	-
0.990	2,782,131.2455	3,181,939.5500	-	-	-

3.1.3 Pressure Validation In Domain

Validation of the pressure is carried out in a domain between a double wall as shown in figure 3.2. Pressure field in the domain as a result of particle motion is computed using equation 2.6. Non-dimensional pressure is defined to be $p^* = \left(\Delta \mathrm{PH}/\mu \mathrm{u}_\mathrm{x}^\mathrm{B}\right)$ where H is the half the height of the channel, and $\mathrm{u}_\mathrm{x}^\mathrm{B}$ is particle's rigid body velocity in horizontal direction. Mesh used in this benchmark is same as that of problem presented in section 3.1.2.

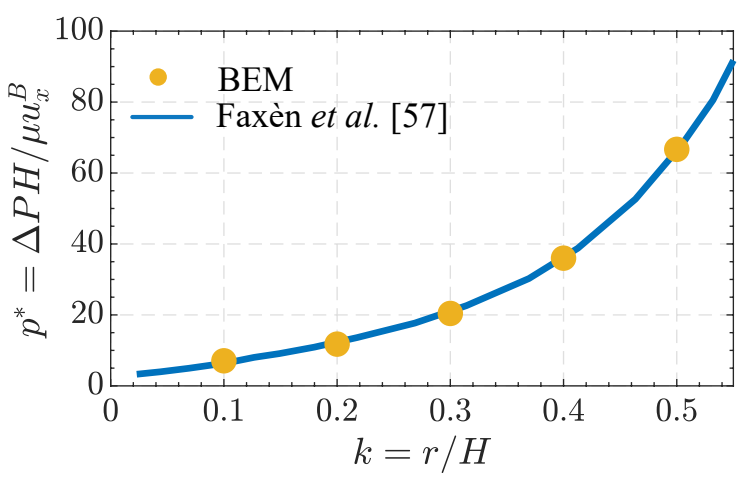

Figure 3.3: Schematics of the benchmark problem for pressure

3.2 Electrokinetic Benchmarks

The main objective of this thesis is to develop and formulate a boundary element based solver to simulate electrokinetic phenomenon for microfluidic applications regarding multi-particle colloidal aggregation. In order to realize that, verification of the hydrodynamic part is not sufficient. The verification of the results of electrical field under different settings is a necessity. For the electric field problem, two separate cases are considered. Firstly, the particle behavior next to a non-conducting wall and secondly particle behavior in the vicinity of an anode is investigated.

3.2.1 Electric Field Parallel to a Wall

As opposed to the pure hydrodynamics, the translational velocity and the rotation of the particle increases without a bound if particle approaches to the wall in electrokinetics. This behavior obtained by BEM and the qualitative comparison between the analytical solution could be seen in figure 3.5. In this setting, the presence of the particle induces a tangential electric field on the wall, which results in a slip velocity with a high magnitude compared to far ends of the wall. Due to magnitudal difference of slip velocities between the top and bottom part of the particle, total torque on the particle becomes non zero. As a result, particle rotates in counter-clockwise direction.

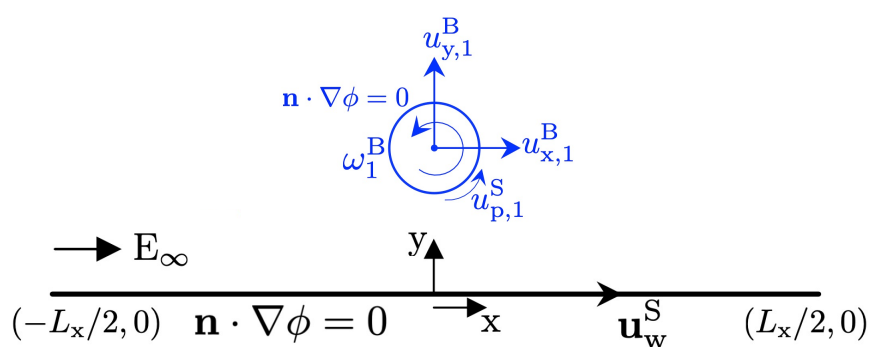

Figure 3.4: Schematics of the EK benchmark problem near a conducting wall

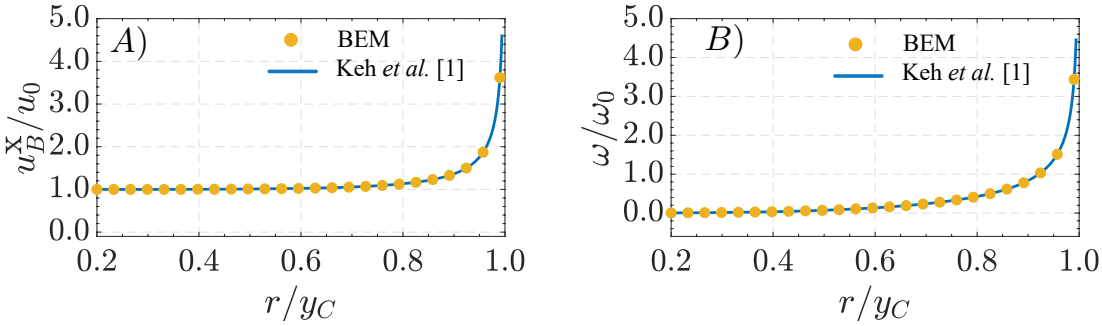

Figure 3.5: a: Comparison of non-dimensional horizontal velocity b: comparison of non dimensional rotational velocity with respect to analytical solution

Dustin *et al.* [60] also studied the same problem using BEM. They utilized circular elements to capture the geometry of the particle and constant functions for field variables over the elements. Throughout the simulations in order to be able to make a meaningful comparison, similiar mesh structure was utilized. Thus, 256 uniform elements on a particle with a radius of 2.5 μm and 192 non-uniform elements on the wall with a length of 30 times particle's radius was used. In table 3.3, a numerical comparison between quadratic-quadratic BEM (present study), circular-constant BEM and analytical solution proposed by Keh *et al.* [30] is given. As expected, present study is superior over circular-constant formulation due to its improved accuracy.

Table 3.3: EK velocity comparison between present study (PS), Dustin *et al.* [60] and the analytical solution given by Keh *et al.* [30].

	Present Study (PS)		**Results From [60]**		**Keh *et al.* [30]**		**Error [%]**	
$\mathbf{r/y_C}$	$\hat{\mathbf{U}}_\mathbf{p}$	$\hat{\mathbf{w}}$	$\hat{\mathbf{U}}_\mathbf{p}$	$\hat{\mathbf{w}}$	$\hat{\mathbf{U}}_\mathbf{p}$	$\hat{\mathbf{w}}$	$\hat{\mathbf{U}}_\mathbf{p}$	$\hat{\mathbf{w}}$
0.20	1.0001	0.0041	1.0000	0.0041	1.0002	0.0041	0.0132	0.7746
0.60	1.0244	0.1351	1.0244	0.1351	1.0250	0.1350	0.0553	0.0605
0.80	1.1328	0.4268	1.1328	0.4267	1.1333	0.4267	0.0508	0.0256
0.90	1.3648	0.8362	1.3648	0.8360	1.3650	0.8362	0.0190	0.0033
0.95	1.7577	1.3726	1.7577	1.3720	1.7574	1.3729	0.0164	0.0212
0.98	2.6137	2.3639	2.6120	2.3620	2.6121	2.3648	0.0608	0.0378
0.99	3.6188	3.4373	3.5963	3.4464	3.6149	3.4391	0.1069	0.0557

3.2.2 Electric Field Perpendicular to Wall

The change of the type of the wall results in an alteration in the flow dynamics. Next to a conducting surface (i.e. an electrode), particle approaches to the wall provided that the particle carries counterion charges. Due to the symmetry of the configuration, a colloidal particle does not rotate. Therefore, verification for the rotation of a cylindrical particle is not considered in the vicinity of a conducting surface. The analytical solution for this problem is given by Keh *et al.* [31]. In their solution, they proposed a *Dirichlet* boundary condition such that ζ_{w} is zero on the planar boundary. As a result, no slip velocity occurs on the surface of the electrode. The electrophoretic velocity of the particle approaches to zero as the distance between electrode and the electrode diminishes and particle comes to a stop. In this benchmark, the same mesh as that of in first electrokinetic benchmark (non-conducting wall) was used. Throughout the simulations an error of 0.1% was achieved at the distance of as close as 5 nm to the wall.

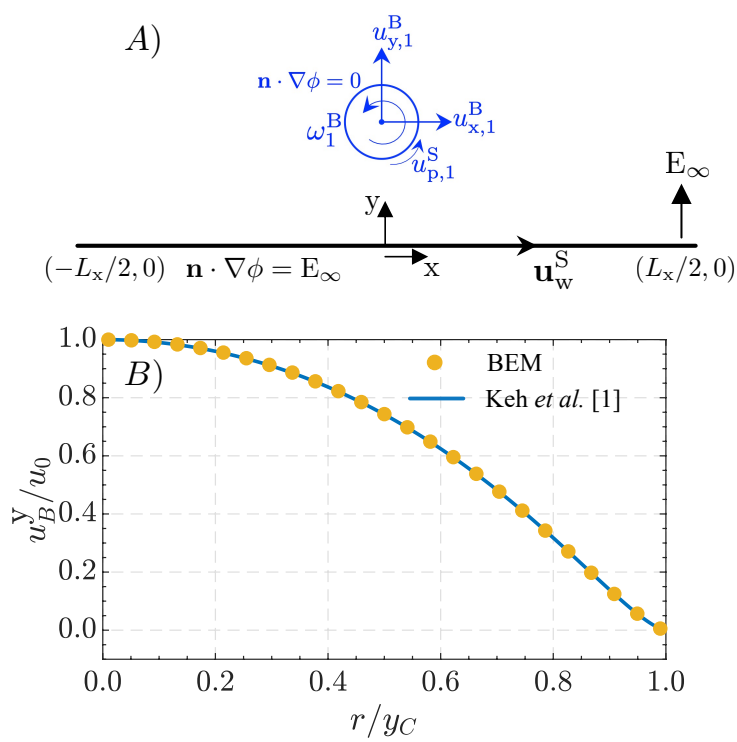

Figure 3.6: a: Schematics of the benchmark problem near a conducting wall, b: Comparison of non-dimensional velocity between present study and analytical solution

3.2.3 Validation of Electric Field

The potential distribution in a 2-D domain is governed by Laplace's partial differential equation as it is seen in equation 3.5.

$$\frac{\partial^2 \phi}{\partial \mathrm{x}^2} + \frac{\partial^2 \phi}{\partial \mathrm{y}^2} = 0 \tag{3.5}$$

An analytical solution to 2-D Laplace equation with four boundary conditions ϕ(x,0) = 0, ϕ(0,y) = 0, ϕ(x,h) = ϕ_o, ϕ(w,y) = 0 exists for a 2-D domain where the domain dimensions w and h are of unit length such that:

$$\phi(x,y)/\phi_o = \frac{4}{\pi} \sum_{k=1}^{\infty} \frac{\sin\Big((2k-1)\pi\,(x/w)\Big)\sinh\Big((2k-1)\pi\,(y/w)\Big)}{(2k-1)\sinh\Big((2k-1)\pi\,(h/w)\Big)} \tag{3.6}$$

The electric field obtained from such potential distribution is given as:

$$\mathrm{E_x} = -\frac{\partial \phi(\mathrm{x},\mathrm{y})}{\partial \mathrm{x}}, \qquad \mathrm{E_y} = -\frac{\partial \phi(\mathrm{x},)}{\partial \mathrm{y}}, \qquad |\mathbf{E}| = \sqrt{\mathrm{E_x^2} + \mathrm{E_y^2}} \tag{3.7}$$

In figure 3.7a, non-dimensional potential distribution in a 2-D domain is presented. In figure 3.7b, the magnitude of the electric field obtained by BEM is compared with analytical solution along the line passing through the points (0.5, 0.0) to (0.5, 1.0). It is seen that the BEM results are in accordance with analytical solution.

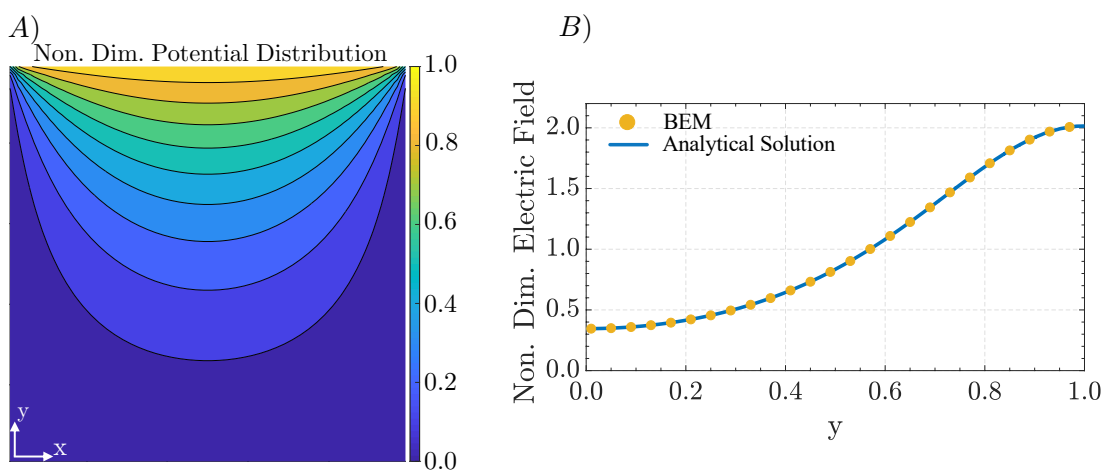

Figure 3.7: a: Non-dimensional potential distribution in the domain, b: Non-dimensional electric field comparison in a square domain

Chapter 4

EK Motion of Colloidal Cylinder(s)

4.1 Conducting Wall

The simulation parameters can be summarized as follows: $\rho = 1000\,\mathrm{kg/m^3}$, $\mu = 10^{-3}\,\mathrm{Pa{\cdot}s}$, $L_\mathrm{x} = 50D$, $a_1 = a_2 = D/2 = 5\,\mu\mathrm{m}$, $\mathrm{E}_\infty = 0.6\,\mathrm{V/cm}$, $\zeta_\mathrm{P}^1 = \zeta_\mathrm{p}^2 = -25\,\mathrm{mV}$, $\zeta_\mathrm{w} = +100$ mV, $\varepsilon_m = 80\varepsilon_o$, $c_\infty = 0.15$ mM, $n_\infty = c_\infty \times (1000N_A)$, where N_A is the Avagadro's number. The velocity of the particle scaled with the EP velocity in an unbounded flow, $u_o = -(\varepsilon\zeta_\mathrm{P}/\mu)E_\infty$ (which is equal to 1.19 μm/s in our simulations). In the simulations, non-uniform elements are utilized to resolve to extremely narrow gaps. For the simulations with 180 and 360 second-order isoparametric elements are implemented on the particles and on the wall, respectively. Numerical integrations are performed using Gauss-quadrature with 20 points and singular integrals are evaluated numerically following the algorithm given in [61], details of the transformation is shared in Appendix B.

Boundary conditions for a conducting wall are modified as appropriate to *disturbance based* single-wall formulation. The potential is separated into two sub-components: background potential and disturbance potential due to presence of the particle as shown in equation 2.7. Due to presence of EDL, electrical boundary condition on the particle is a homogenous Neuman boundary condition:

$$\mathbf{n} \cdot \nabla\phi = 0 \tag{4.1}$$

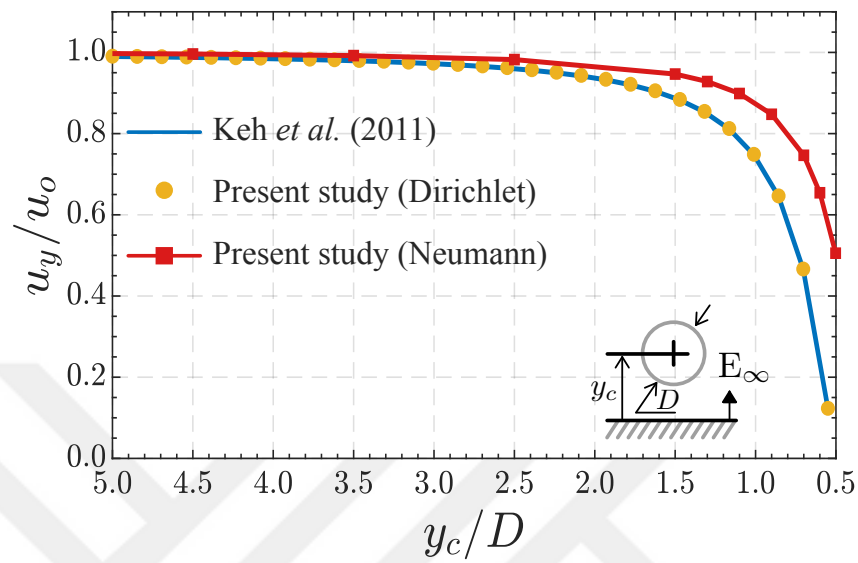

Figure 4.1: Comparison of the present study with the analytical solution given by Wang and Keh for the case of single particle near a conducting wall with Dirichlet boundary condition, and the result of the present study with the Neumann boundary condition.

note that $\mathbf{n} \cdot \nabla\phi = 0$ due to boundary condition shown in equation C.1. provided that the electric field is in y direction. As for the Stoke's boundary conditions, slip boundary conditions on the particle become:

$$\mathbf{u}_{\mathrm{p}}^{\mathrm{S}} = \frac{\varepsilon_m \zeta_{\mathrm{p}}}{\mu} (\mathbf{I} - \mathbf{nn}) \cdot \nabla\phi \tag{4.2}$$

Regarding the slip velocity on the wall, in order to obtain disturbance velocity the following is made:

$$\mathbf{u}_{\mathrm{W}}^{\mathrm{D}} = \mathbf{u}^{\mathrm{S}} - \mathbf{u}^{\infty} \tag{4.3}$$

Note that in this case, there are no vertical walls. Thus, there is no background flow in the vertical direction. For the completeness purposes however, $\mathbf{u}^{\infty}$is included in notation. As a result,

$$\mathbf{u}_{\mathrm{W}}^{\mathrm{D}} = \frac{\varepsilon\, \zeta_{\mathrm{w}}}{\mu} (\mathbf{I} - \mathbf{nn}) \cdot \nabla\phi^{D} \tag{4.4}$$

The analytical solution to this problem was first given by Wang and Keh [31]. In this configuration, Dirichlet boundary condition was considered which

results in zero slip on the surface of the electrode. Therefore, the only mechanism responsible for particle motion was the EP of the particle under externally applied electrical field. DEP force was also ignored in that study. As a result of the zero slip on the electrode surface, the EP velocity of the particle diminishes to zero as the particle approaches to the boundary. Since there is no pressure contribution from the wall, the distance between the particle surface and electrode becomes as small as 1% of the radius of the particle. The same configuration is also simulated using a Neumann boundary condition on the electrode which is a more realistic boundary condition for a conducting wall, as discussed in the introduction section. Simulation results describing particle behavior under Neuman boundary condition could be seen in figure 4.1. With the implementation of the Neuman boundary condition, the slip-velocities present themselves on the wall which also affect the slip-velocities on the particle surface. As a result of this interaction, it can be clearly observed that the particle velocity reaches to a value that is half of the EP velocity in an unbounded flow even for very small particle-wall spacing. The slip velocities on the wall are responsible for hydrodynamic pressure accumulation below the particle. Thus, particle comes to a stop at a certain location, which is considerably farther than Dirichlet case. In the case of Dirichlet boundary condition, there is no pressure contribution from the wall. Thus, particle reaches as close as 5nm to the wall.

In single-particle simulations, a particle is released from a distance of five diameters away from the wall. Having been subjected to sedimentation under gravitational acceleration until the distance between the particle and electrode reached to four diameter, the DC electric field is activated. As the field is activated, a jump in the total velocity of the particle is observed. The results are expressed in non-dimensional form where electric potential and time are normalized with $\phi_o = \mathrm{E}_\infty \cdot \mathrm{D}$ and $t_o = \mathrm{D}/\mathrm{u_o}$, respectively. In Fig. 4.2, the particle position and y–velocity are shown. Contributions of different external forces (referring to Eq. (2.18)) are also presented separately in the figure with the exception of colloidal forces which are negligible in this case. As can be depicted from Fig. 4.2, the EK velocity presents itself once the electric field is activated, and the contribution of the wall comes into the picture approximately 2 diameters away

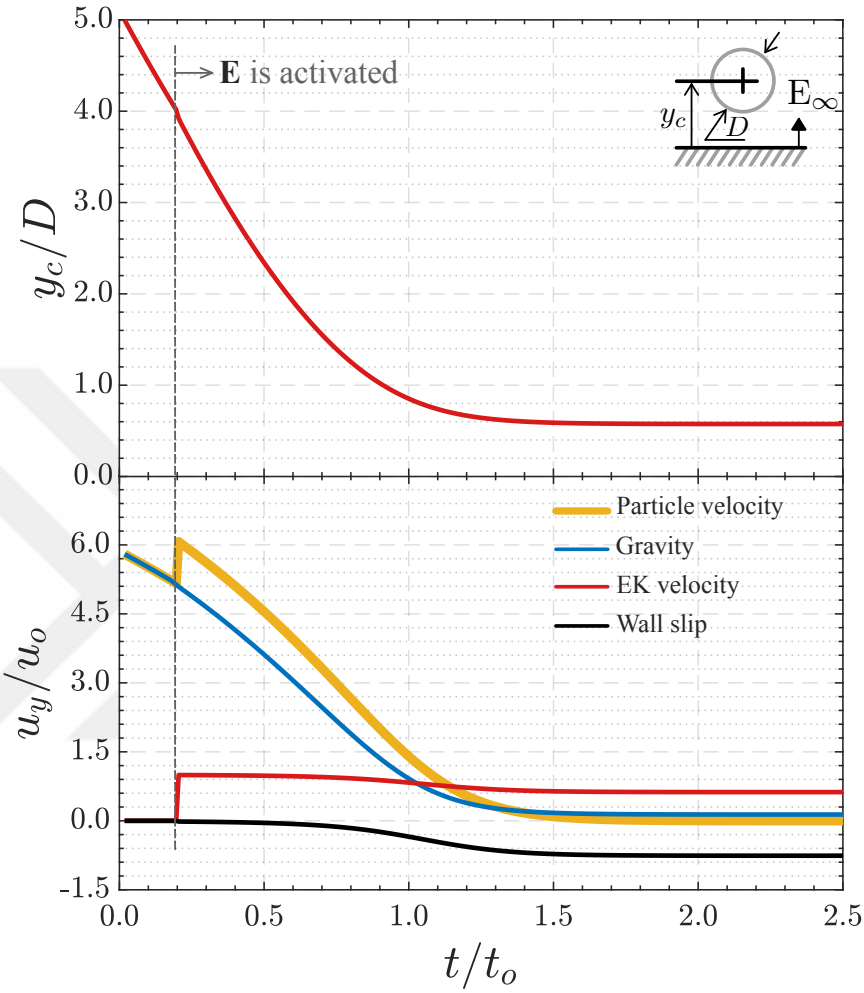

Figure 4.2: The position and velocity of a particle in the y–direction as it moves towards the wall. The contributions of different physical phenomena on the velocity are shown separately.

from the wall, and acts in the opposite direction of the sedimentation velocity. Since the contribution of the wall increases as the particle is approaching to the wall, the particle eventually reaches to an equilibrium height, when the distance between the particle center and the wall is about 0.6D (This leaves 0.1D distance between the bottom of the particle and the wall).

Figure 4.3 illustrates the electric field and streamlines with the electric potential and pressure field contours at three different instances during the particle motion. The corresponding wall electric potential and the slip-velocity on the

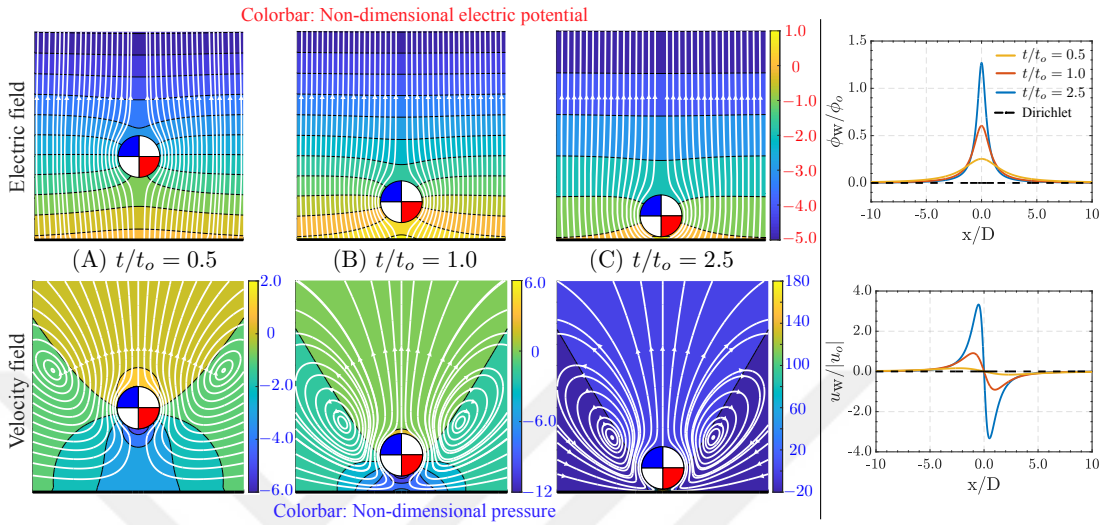

Figure 4.3: Flow and electrical fields around a particle as it moves towards the wall. Electric field lines and the streamlines are shown. Background color corresponds to non-dimensional electric potential and non-dimensional pressure distribution, respectively. The right column shows the non-dimensional wall potential and wall slip-velocity at different times.

wall are also shown in the last column of the figure. The results are given in non-dimensional form where the pressure is normalized by the viscous forces ($\mu u_o/D$). Owing to the implementation of the Neumann boundary condition on the electrode, presence of the particle near the electrode disturbs the electrode potential and creates slip velocity on the electrode's surface. Electric field lines near the particle induces slip velocity on the particle that results in the formation of a symmetric recirculating flow pattern as shown in the lower figures. Particle wall interactions increase as the particle gets closer to the electrodes, and the strength of the circulation increases. Moreover, pressure builds up underneath the particle. The presence of the circulating cell at both sides of the particle near a conducting wall is an observed phenomena in the literature [27–29, 33, 34]. In addition, the pressure build up is also discussed by Yariv [29], who performed near contact analysis for a spherical particle near a conducting wall.

Although the contribution of DEP and EP are included in the EK formulation, the DEP force has negligible effects for the single-particle case in x–direction due to symmetry of the problem. On the other hand, although the presence of the

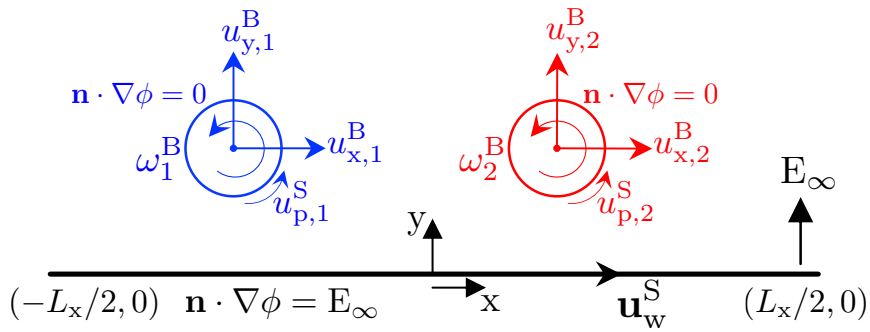

Figure 4.4: Schematic description of multi-particle problem next to a conducting wall

wall creates a gradient also in the y–direction, the effect of DEP is again negligible compared to the other contributions. This finding significantly differs from the case of electric field parallel to a non-conducting wall studied in [15], where the particle motion and its equilibrium position were shown to be greatly effected by DEP.

Multiple particles electrophoretically deposited onto a substrate using DC or low frequency electric fields show particle aggregation. This experimentally observed behavior is quite unexpected considering the Coulombic and induced-dipole repulsion effects [62]. Particle aggregation takes place even for particles separated by five diameters. To demonstrate this physical phenomena, two-particle simulations are performed. Two particles are released five diameters above the wall and six diameters away from each other. Similar to the single-particle simulation, the particles are allowed to sediment under gravity until they are four diameters above the wall, and then the DC electric field is applied. Non-dimensional position and velocity of the particles in x– and y–directions are shown in Fig. 4.5. The particles sediment onto the electrode surface quite fast and then they quickly reach their equilibrium position in y–direction. However, the particle motion and the time for reaching the equilibrium position in x–direction take longer. In the bottom row of the figure, we show the particle velocities as a function of time in both directions. However, we specifically focus on the initial process during the sedimentation, where an equilibrium position in $y-$ direction is determined, and the final moments before an equilibrium in the horizontal direction is established. As seen from the figure (right panel), the particles initially

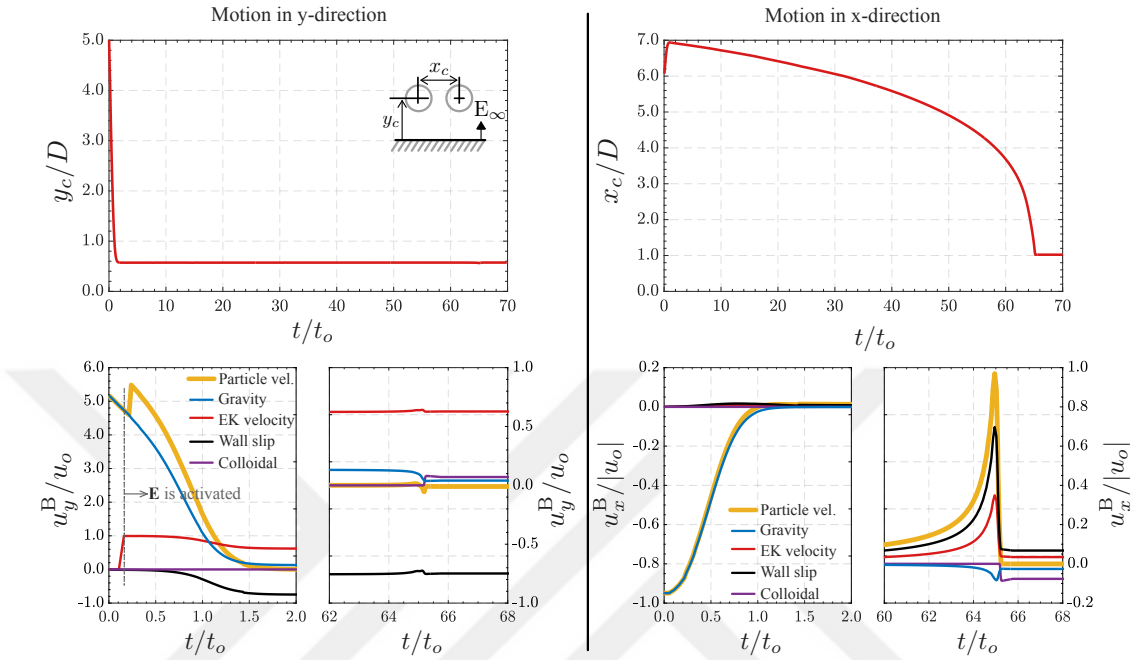

Figure 4.5: The position and velocity of multiple particles in the y–direction and x–direction as they move towards the wall. The contributions of different physical phenomena on the velocity are shown separately.

start at a separation distance of six diameters and repel each other up to about seven diameters under gravitational and EP forces. This is followed by particle-particle attraction due to the induced slip-velocity on the wall, and hence, the induced vortices. Eventually, the distance between the particles reaches almost a diameter, which is the touching condition. To be exact, the centers of the particles reach equilibrium distances of $1.02D$ and $0.57D$ in the horizontal and vertical directions, respectively. Especially, the inter-particle colloidal force component, which did not play a role in the single particle-case, becomes important in the multi-particle case. The colloidal force between the particle and the wall also affects the motion in $y-$ direction; however the effect is not as significant as that in $x-$ direction. Actually, when the colloidal forces come into the picture, a new equilibrium both in the horizontal and vertical directions are achieved. Another important observation is that the contribution from the wall slip pushed the particles away from the wall and this contribution results in repulsive motion in the $x-$ direction. The contribution of the gravity has a similar behavior. Gravity

causes a downward motion which induces an attractive motion in the horizontal direction. A peculiar behavior here is the sudden decrease of the velocities at about non-dimensional time of 65. To further discuss this point, we need to observe the wall potential and the wall slip about that point.

Figure 4.6 shows the electric field lines and the streamlines with the electric potential and pressure field contours. The corresponding wall electric potential and the slip-velocity on the wall are also shown in the right column of the figure. Once the particles come closer to the wall, the slip-velocity on the wall generates vortices which move the particles towards each other. As the particles come closer, the vortices occurring between the particles lose their strength and disappear when the particles are very close to each other. As seen from the pressure field, although pressure build up is observed underneath each particle when they are away from each other, a negative pressure is realized between the two neighboring particles at close proximity with a circulation region between them. Actually, the disturbance of the electric potential and slip-velocity on the electrode's surface are amplified compared to that of single-particle. Therefore, the presence of the second particle has great impact both on the electrical field and the flow field. At this point, the origin of the interesting behavior at about non-dimensional time of 65 can be understood. As seen in the last column, the disturbance of the electric potential and slip-velocity on the electrode's surface increases as the particles comes closer, and actually when non-dimensional time is 65.5, the wall potential has a single maxima instead of two-humps, which also manifest itself as single maxima and minima for the wall slip-velocity. As the wall slip-velocity increases, the contribution of the wall slip on the particle velocity enhances and so does the EK contribution due to the amplified local electric field around the particle (please see Fig. 4.5). Then, when the particles come to a certain distance the EDL contribution takes over and cause a sudden stop of the particles. One may think that sudden stop of the particles is nonphysical. However, the EDL force is highly nonlinear and has hyperbolic behavior due to the polylogarithmic function. The colloidal interaction force increases exponentially after a certain threshold distance. At this point, the wall slip-velocity still exists and causes two small vortices underneath the particle. Vortex between the two particles die

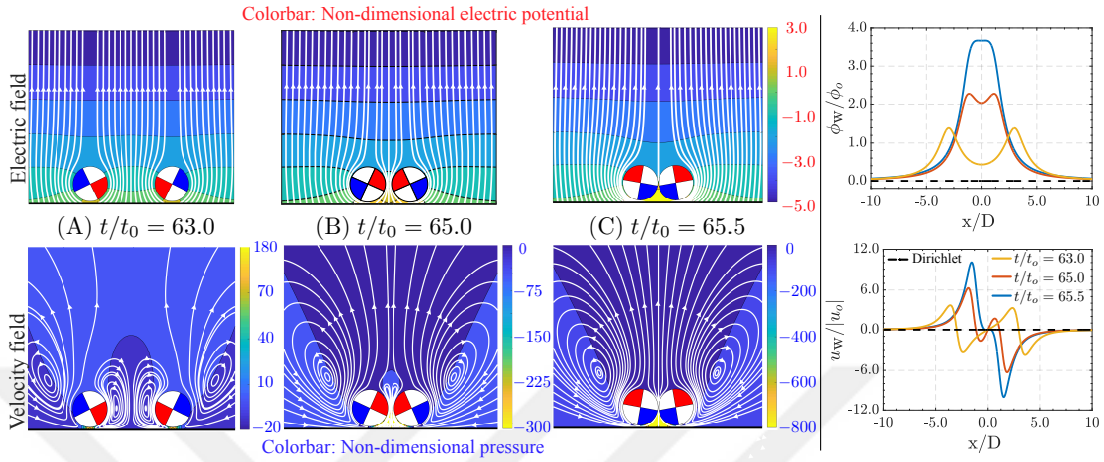

Figure 4.6: Electric field lines and streamlines at three different instances during the two-particle motion. Non-dimensional electric potential and pressure field contours are also shown in the background. The right column shows the non-dimensional potential and slip-velocity on the electrode's surface at three distinct times.

out after certain proximity, and this leads to a negative pressure field in that region. We would like to also mention that although the contributions of DEP and EP are given in EK, and the contributions of EDL and vdW are given in the colloidal component, the DEP (the ratio of DEP/EP is about 5%) and vdW (the ratio of EDL/vdW is about 10%) have negligible effects for the multi-particle case. At the equilibrium point, results yield that vdW contribution constitutes one tenth of EDL contribution, while DEP constitutes one percent of the total EK contribution. The comparison of the single-particle and two-particle cases also reveal stronger disturbance and wall slip-velocity that results in stronger circulation for the two-particle case. This means that a two-particle pair would attract other neighboring single particles that are farther away form the couple, and the particles will rapidly aggregate, as shown in previous experimental results [8].

Although it is not presented here, the equilibrium positions for smaller particles with a diameter less than 5 μm become very small which invalidates our thin EDL and pairwise interaction approach for the three-body problem, and for some cases, we reached touching condition which was also observed in the previous experiments with DC fields [1].

4.2 Non-Conducting Wall

In the vicinity of a non-conducting wall, behavior of colloidals significantly change in comparison to that of colloidal particles' near a conducting wall due to different settings. Since there is no risk of a Faradaic Reaction in the vicinity of a wall, the electric field applied is greatly higher in magnitude. Figure 3.4 depicts the schematics of the problem. In this part of the thesis, the effect of diameter to the equilibrium position is investigated for single particles. For this reason, three different diameters are proposed. Simulation parameters for EK behavior of particles in the vicinity of a non-conducting wall are summarized as follows: $\rho = 1000\,\mathrm{kg/m^3}$, $\mu = 10^{-3}\,\mathrm{Pa{\cdot}s}$, $\mathrm{L_x} = 150\mathrm{D}$, $\mathrm{a_1} = 2.5\mu\mathrm{m}$, $\mathrm{a_2} = 5\mu\mathrm{m}$, $\mathrm{a_3} = 7.5\mu\mathrm{m}$, $\mathrm{E}_\infty = 20\ \mathrm{V/cm}$, $\zeta_\mathrm{P}^1 = \zeta_\mathrm{p}^2 = -25\,\mathrm{mV}$, $\zeta_\mathrm{w} = -31\ \mathrm{mV}$, $\varepsilon_m = 80\varepsilon_o$, $c_\infty = 1\ \mathrm{mM}$, $n_\infty = c_\infty \times (1000 N_A)$, where N_A is the Avagadro's number. The velocity of the particle is scaled with the EP velocity in an unbounded flow, $u_o = \varepsilon\,(\zeta_p - \zeta_w)\,\mathrm{E}_\infty/\mu$.(which is equal to 9.15 μm/s in our simulations). Boundary conditions for a conducting wall are modified as appropriate to *disturbance based* single-wall formulation. Note that potential is separated into two sub-components: background potential and disturbance potential due to presence of the particle as shown in equation 2.7. Due to presence of EDL, electrical boundary condition on the particle and on the wall is a homogenous Neuman boundary condition:

$$\mathbf{n} \cdot \nabla\phi = 0 \tag{4.5}$$

As for the Stoke's boundary conditions, slip boundary conditions on the particle become:

$$\mathbf{u}_\mathrm{p}^\mathrm{S} = \frac{\varepsilon_m \zeta_\mathrm{p}}{\mu}\,(\mathbf{I} - \mathbf{nn}) \cdot \nabla\phi \tag{4.6}$$

Regarding the slip velocity on the wall, in order to obtain disturbance velocity following subtraction is done:

$$\mathbf{u}_\mathrm{W}^\mathrm{D} = \mathbf{u}^\mathrm{S} - \mathbf{u}^\infty \tag{4.7}$$

As a result slip velocity on the wall due to presence of the particle became,

$$\mathbf{u}_\mathrm{W}^\mathrm{D} = \frac{\varepsilon\,\zeta_\mathrm{w}}{\mu}\,(\mathbf{I} - \mathbf{nn}) \cdot \nabla\phi^D \tag{4.8}$$

Detailed information regarding boundary conditions on the particle and planar boundary surface's is explained in Appendix C. In single particle simulations, a particle is released from a distance of one diameter away from the wall. The results are again expressed in non-dimensional form where EP velocity of the particle in a free space and dimensional time is expressed in the form of: $u_o = \varepsilon\left(\zeta_p - \zeta_w\right)\mathrm{E}_\infty/\mu$, $t_o = D/u_o$.

As opposed to the conducting wall case, the background flow exists and is in the direction of the external electric field. The EK velocity of the particle is also in x− direction. Therefore, there is neither EK velocity contribution nor wall contribution in y− direction to the particle velocity. In the beginning, particle moves in horizontal direction due to applied external electric field and descends due to gravitational acceleration. Since the applied external electric field is high in magnitude, the DEP force acts to stop the particle from reaching the wall. Similiar to the foundings of Li *et al.*, [15], as the diameter of the particle increases, the non-dimensional equilibrium position of the particle decreases. Since the EK behavior of such a colloidal is of similiar characteristics with that of colloidals having different diameters, only a single figure for a single particle with a diameter of 15μm is shown, as in figure 4.7.

In figure 4.7 on the first column the vertical location for the center of gravity and the velocities are given. On the second column, the horizontal location of center of gravity and the velocity components are shown. Particle velocity is composed of two independent factors: the summation of the background flow with EK-slip velocities on particle (EK Velocity) and EK slip velocity on the wall (Wall slip). Background flow and wall-slip are in the direction of the applied electric field. Due to the ξ_p value of the colloidal, the electrokinetic slip velocities direct particle in opposite the direction of the applied electric field. As the particle approaches to the wall, due to particle presence, wall-slip contribution is increased.

In table 4.1, gravity, colloidal and DEP induced non-dimensional velocities are shown for colloidals having various diameters ranging from 5μm to 15μm.

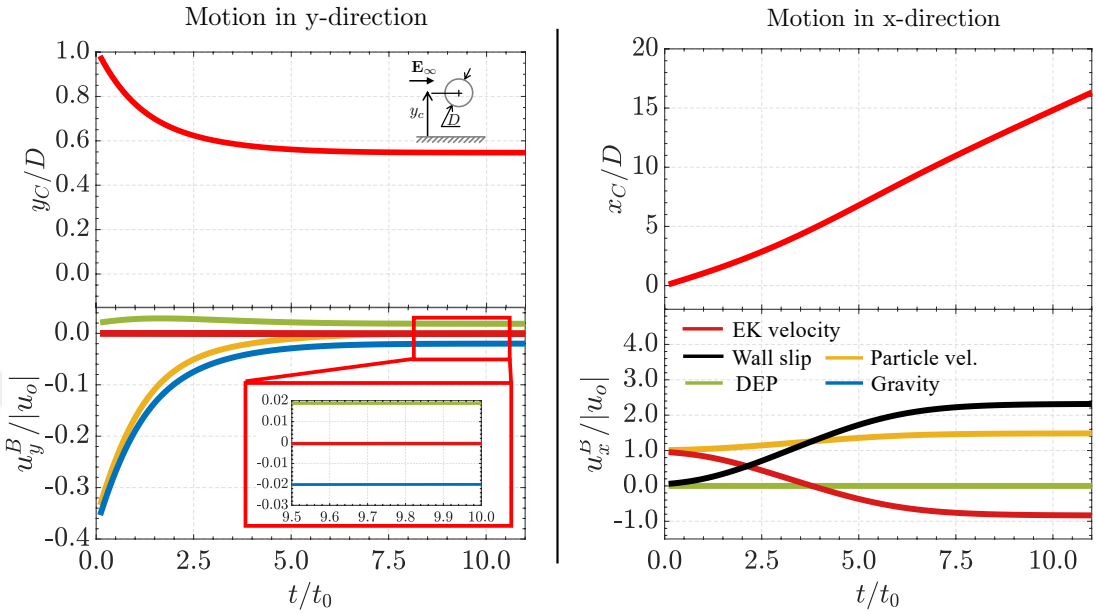

Figure 4.7: Non-dimensional velocities of a single particle in the vicinity of a non-conducting wall for a particle whose diameter is 15μm.

Overall, as the diameter of the particle is increased, the non-dimensional equilibrium position of the particle is decreased. Due to an increased volume of the particle, the non-dimensional velocity contribution due to the gravitational acceleration is increased as well. Particle diameter also affects the DEP contribution as well. As the particle size increases, total DEP force acting on the particle increases, which yields a higher DEP induced velocity contributing to over-all particle velocity. As the particle becomes larger, velocity component due to DEP contribution becomes comparable with velocity component due to gravity and colloidal interactions become negligible for an electric field of 2kV/m.

Table 4.1: Velocity components for colloidals with different diameters

D [μm]	$\mathbf{y_C}$[μm]	**Vertical Velocity [μm/s]**			**Horizontal Velocity [μm/s]**	
		$u_y^{B,GRA}$	$u_y^{B,COL}$	$u_y^{B,DEP}$	$u_x^{B,EK}$	$u_x^{B,Wall}$
5	3.0730	−0.0686	0.0165	0.0833	−3.4102	6.7911
10	5.7251	−0.1491	0.0068	0.1418	−1.2316	13.6152
15	8.1990	−0.1821	0.0068	0.1711	−7.6320	21.2079

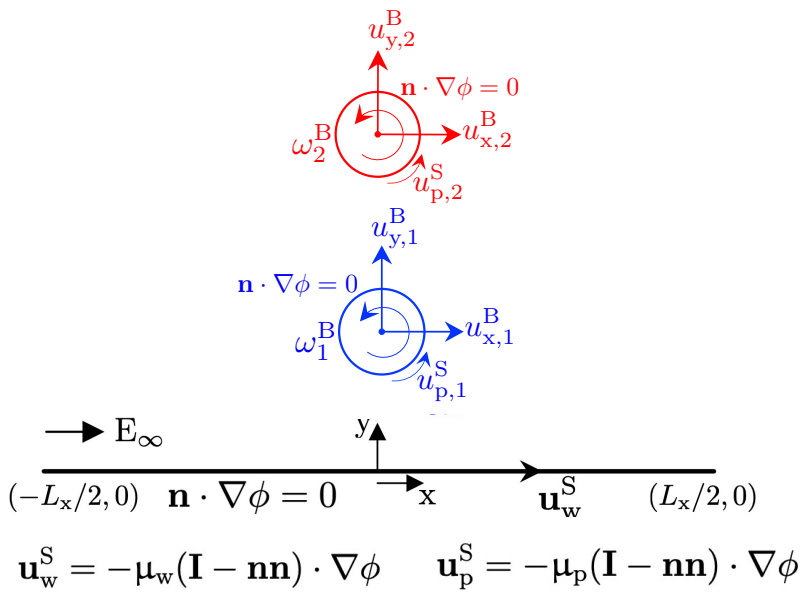

Figure 4.8: Schematics of two particle problem near a non-conducting wall

In multi-particle configuration for colloidals next to a non-conducting wall, two particles (particle number one is placed below particle two) are placed vertically as it is seen in figure 4.8. Particles are initially released from 1D away from the wall, since the wall has no effect on the colloidal behaviour before ≈ 0.7D, as it is seen in figure 4.7. Two particles are then subjected to gravitational acceleration. Unlike single particle case, gravity-induced velocities of particles in -y direction are different due to different initial positions. Thus, the vertical gap between two particles diminishes briefly. In this configuration, it is known that as the particle approaches to the boundary, slip velocities occuring on the wall is going to create a torque on the particle, which results in a higher translational and rotational velocities on the particle boundaries compared to those farther away from the wall. In figure 4.9, the vertical and horizontal locations and velocities for the first particle are given. As it is seen on the left column, as the particles come closer in the vertical direction, particle-particle interactions come into play at around a non-dimensional time of 2. Before particle-particle interaction occurs, DEP acts to stop particle from approaching wall similiar to case for single particle. With the arrival of the second particle, variation of electric field in the domain yields an interesting phenomenon.

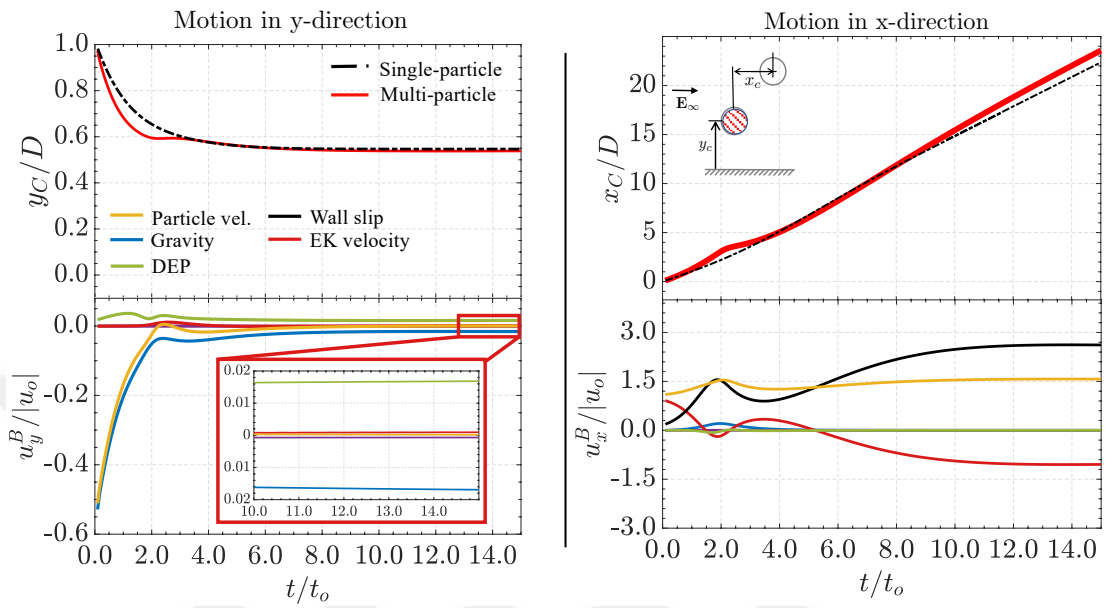

Figure 4.9: Vertical and horizontal velocities of the first particle with a diameter of 15μm

DEP forces in both x− and y− direction decrease between time 1.5 to 2.5 due to non-uniform electric field around the particles. DEP forces acting on the particles as a function of time is shown in figure 4.10. For the first particle, vertical velocity values based on DEP contribution decrease in magnitude, due to a decrease in DEP force in y− direction. In the mean time, EK slip velocities act to attract particles. This could be seen at around non-dimensional time of 2.1 at which total particle velocity becomes positive. In the horizontal direction, wall slip reaches to its maximum value at non-dimensional time of 2. After that time, even though

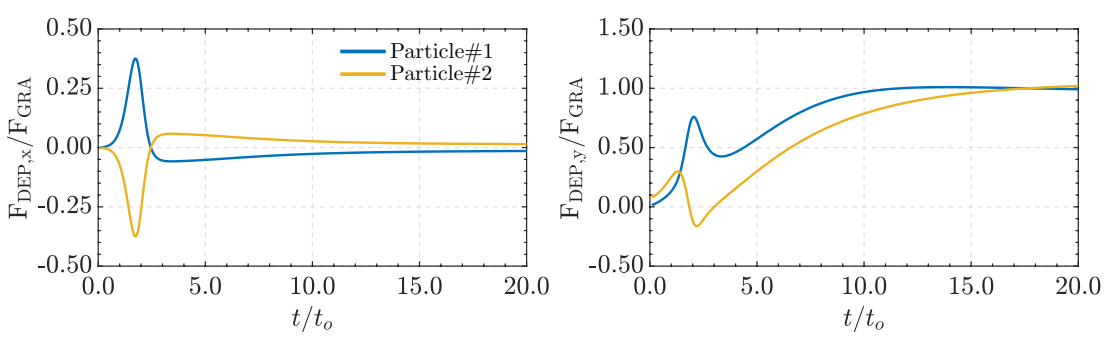

Figure 4.10: DEP forces in x− and y− directions throughout the simulations for the particles with a diameter of 15μm

for a short duration, particle moves away from the wall. Thus, wall-slip and EK velocity contribution decrease. The sign of surface potential of the particle (ξ_p), yields such an EK slip velocity on the particle that it directs particle towards the source of the external electric field. On the other hand, the background flow acts on the particle in the direction of the external electric field. Since EK velocity in figure 4.9, consists of both slip velocities on the particle and the effect of background flow, initially EK velocity is positive, which means, background flow is dominant over slip velocities on the particle. However, as particle approaches to the wall, EK slip on the particle becomes higher in magnitude and wins over background flow. This is why there is a sign change in the values for EK velocity contribution. Then particles reach an equilibrium and continue their movement. All in all, due to particle-particle interactions, first particle approaches to wall much faster compared to single particle case.

Concerning the behavior of the second particle, as it is seen in figure 4.11, similiar to the first particle, the second particle is also subjected to a positive DEP force during its decline (before non-dimensional time of 2). However, the absence of the first particle beneath the second particle forms a non-uniform electric field and yields an *attractive* DEP force acting on the second particle.

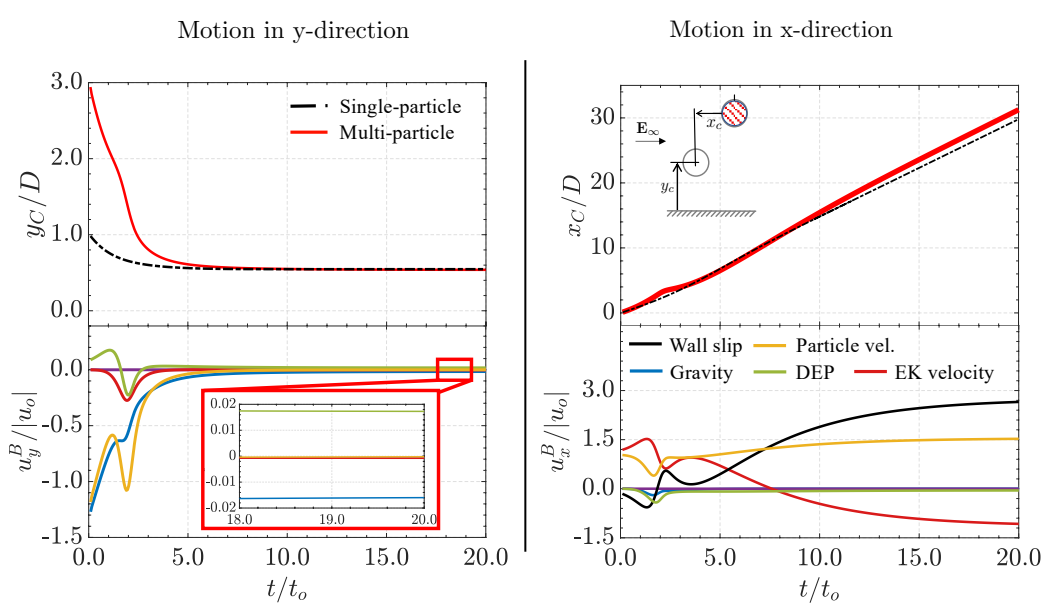

Figure 4.11: Vertical and horizontal velocities of the second particle with a diameter of 15µm

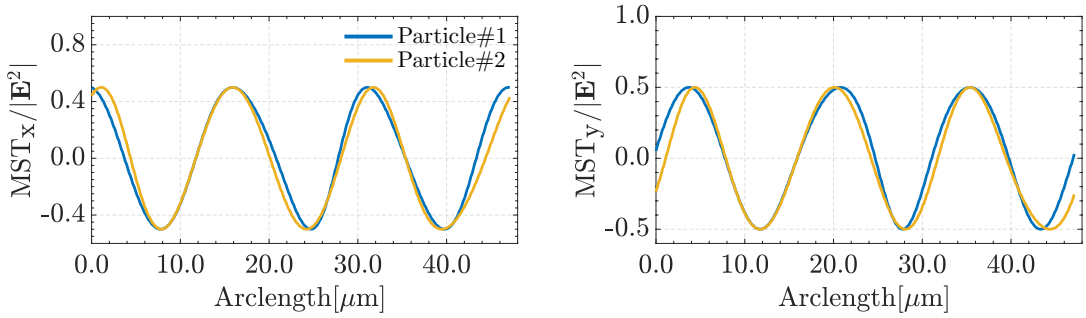

Figure 4.12: Maxwell Stress Tensor (MST) comparison for the particles in the vicinity of a wall

Such an attractive force also produces a rotation in the opposite direction of the first particle. Due to negative DEP, the vertical distance between two particles is covered quickly, which results in a jump in EK velocity both in x− and y− directions. However, because the first particle is closer to wall than the second wall, it moves faster and as the distance between two particles increase, they reach an equilibrium. One could shed a light on the origin of negative DEP force on the second particle by inspecting MST values over the arclength of the colloidals. Integration of MST_y over the surface of the second particle yields a negative force,

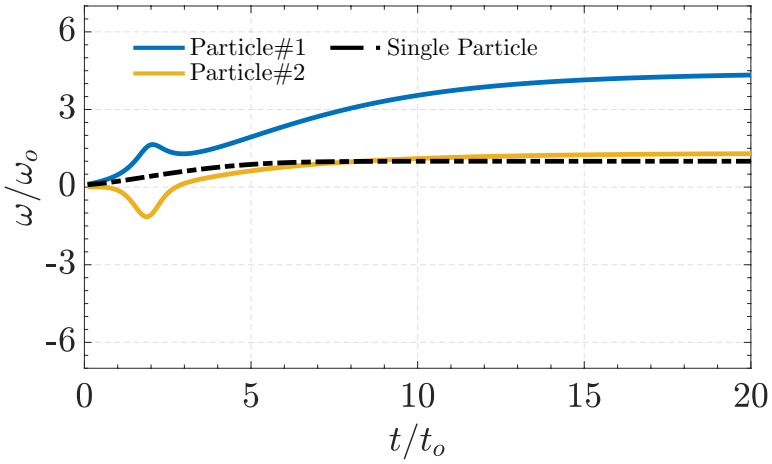

Figure 4.13: Maxwell Stress Tensor (MST) comparison for the particles in the vicinity of a wall

see equation 1.3. On the other hand, such an integration over the surface of the first particle yields a positive value. Non-dimensional rotational velocties of

the particles are depicted in figure 4.13. Due to p-p interaction, initially second particle rotates in clock-wise direction. Then, with the effect of the wall, direction of the rotation changes and as a result converges to single-particle case. First particle, on the other hand is closer to wall and is subjected to extra torque due to presence of the second particle. Thus, has a higher non-dimensional rotation overall.

The non-dimensional potential and electric field around the particles are depicted in figure 4.14. At time $t/t_o = 0$ and $t/t_o = 3.4$ electric field is higher in magnitude than electric field above the particle. However, at time 2.1, electric field below the particle is smaller in magnitude than it is above the particle. Consequently, simulation results revealed that multi-colloidal interactions near a planar wall under various boundary conditions yield intriguing phenomena.

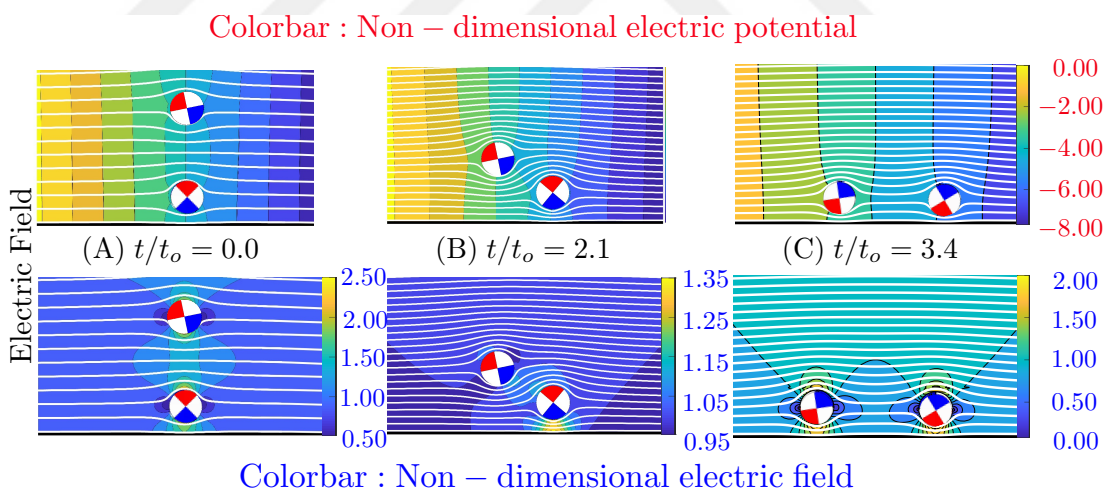

Figure 4.14: Non-dimensional potential and electric field of 15µm particles

Chapter 5

Conclusion and Future Work

Facilitation of the present custom BEM based solver allowed detailed inspection of EK behavior of colloidals as well as interparticle interactions under various boundary conditions and revealed insight regarding colloidal dynamics. In the present study, a series of simulations concerning multi-particle interactions next to a wall were carried out. The investigation of multi-particle interactions in the vicinity of an electrode revealed that external electric field yields an attractive EK colloidal behavior. In addition, the wall contribution plays a prominent role in the aggregation of the colloidals. Considering BEM simulations, it was shown that horizontal velocity of the colloidals is inversely related to surface to surface colloidal distance. Once the colloidals attract each other two vortice between colloidals form, which results in a lower pressure field between colloidals. The shorter the distance between colloidals become, the more rotational and translational velocities increase. As the gap between colloidals diminishes, these vortice wade towards the end of their motion. Finally, colloidal forces halt the motion of particles in horizontal direction. Concerning simulations, it could be concluded that an implementation of *Neuman* boundary condition throughout the simulations is crucial as it is responsible for the formation of electrohydrodynamic flow, which is one of the main mechanisms for the colloidal aggregation.

The investigation of multi-particle interaction in the vicinity of a non-conducting wall revealed that relative positions of colloidals with respect to each other are of considerable importance. As their relative position alters local electrical field such that intriguing DEP related behavior occurs. In this case, alterations in local electric field result in sign changes in DEP forces, which causes formation of both *attractive* and *repulsive* forces. Similiar to the conducting wall case, external electric field results in an attractive EK colloidal behavior. However, in this case, the background flow exists and it is responsible for the motion of colloidals in x− direction. In addition, due to high electric field values throughout the simulations (E_∞ = 20V/cm), particle-particle distances are far enough to prevent colloidal effects from influencing the motion of the colloidals. Consquently, after the interparticle interactions occur, they reach an equilibrium position and continue their movement in x− direction.

Considering all the aspects, the proposed computational model is versatile and robust to investigate the complex colloidal interactions. As for the future research direction, it is aimed to extend the capabillity of BEM code to include AC electric field driven transport of biological cells in 2-D, which includes multi-domain computations. Moreover, the aggregation dynamics of colloidal particles is a richer phenomenon in the case of an oscillating electric field through which the frequency of the field affects the charge dynamics within the EDL. The implementation of the current computational model for the oscillating current will also be one of the future research directions which will be followed by the assessment for non-circular particles. Although qualitative behavior can be predicted by this 2D model, upon the implementation, it is possible to obtain quantitative behavior for 3D colloidal interactions. With this improvement, it will be possible to model electrokinetic behavior of both isotropic colloidals and those having anisotropic surface characteristics such as Janus particles. Therefore, the extension of the current model to 3D problems will be one of the bases for future research direction. Another main objective is to render code suitable for running it in parrallel. Especially for multi particle computations, the parallelization of the code with domain decomposition techniques would shorten overall simulation time.

Bibliography

[1] M. Trau, D. A. Saville, and I. A. Aksay, "Field-induced layering of colloidal crystals," *Science*, vol. 272, no. 5262, pp. 706–709, 1996.

[2] M. Trau, D. A. Saville, and I. A. Aksay, "Assembly of colloidal crystals at electrode interfaces," *Langmuir*, vol. 13, pp. 6375–6381, 11 1997.

[3] E. M. Wong and P. C. Searson, "ZnO quantum particle thin films fabricated by electrophoretic deposition," *Appl. Phys. Lett.*, vol. 74, no. 20, pp. 2939–2941, 1999.

[4] W. D. Ristenpart, I. A. Aksay, and D. A. Saville, "Assembly of colloidal aggregates by electrohydrodynamic flow: Kinetic experiments and scaling analysis," *Phys. Rev. E*, vol. 69, p. 021405, 2004.

[5] T. Gong and D. W. M. Marr, "Electrically switchable colloidal ordering in confined geometries," *Langmuir*, vol. 17, pp. 2301–2304, 04 2001.

[6] W. D. Ristenpart, I. A. Aksay, and D. A. Saville, "Electrically guided assembly of planar superlattices in binary colloidal suspensions," *Phys. Rev. Lett.*, vol. 90, p. 128303, 2003.

[7] O. D. Velev and E. W. Kaler, "In situ assembly of colloidal particles into miniaturized biosensors," *Langmuir*, vol. 15, pp. 3693–3698, 05 1999.

[8] P. Bahukudumbi, *Energy Landscape and Electric Field Mediated Interficial Colloidal Assembly.* Phd dissertation, Texas A&M University, 2012.

[9] Böhmer, "In Situ Observation of 2-Dimensional Clustering during Electrophoretic Deposition," *Langmuir*, vol. 12, pp. 5747–5750, jan 1996.

[10] D. Li, *Preface*, vol. 2 of *Interface Science and Technology*. Elsevier, 2004.

[11] B. Cetin, M. B. Ozer, and M. E. Solmaz, "Microfluidic bio-particle manipulation for biotechnology," *Biochemical Engineering Journal*, vol. 92, pp. 63–82, 2014.

[12] T. M. Squires and M. Z. Bazant, "Induced-charge electro-osmosis," *J. Fluid Mech.*, vol. 509, pp. 217–252, 2004.

[13] B. Cetin and D. Li, "Dielectrophoresis in microfluidics technology," *Electrophoresis*, vol. 32, pp. 2410–2427, 2011.

[14] D. Li, *Electrokinetics in Microfluidics*, pp. 1–5. Elsevier Academic Press, 2004.

[15] E. W. K. Young and D. Li, "Dielectrophoretic force on a sphere near a planar boundary," *Langmuir*, vol. 21, pp. 12037–12046, 2005.

[16] D. House and H. Luo, "Effect of direct current dielectrophoresis on the trajectory of a non-conducting colloidal sphere in a bent pore," *Electrophoresis*, vol. 32, pp. 3277–3285, 2011.

[17] M. Camarda, S. Scalese, and A. L. Magna, "Analysis of the role of the particle-wall interaction on the separation efficiencies of field flow fractionation dielectrophoretic devices," *Electrophoresis*, vol. 36, pp. 1396–1404, 2015.

[18] E. Yariv, "The electrophoretic mobilities of a circular cylinder in close proximity to a dielectric wall," *J. Fluid Mech.*, vol. 804, p. R5, 2016.

[19] E. Yariv, "Dielectrophoretic sphere-wall repulsion due to a uniform electric field," *Soft Matter*, vol. 12, pp. 6277–6284, 2016.

[20] B. Cetin, S. D. Oner, and B. Baranoglu, "Modeling of dielectrophoretic particle motion: Point particle vs finite-sized particle," *Electrophoresis*, vol. 38, pp. 1407–1418, 2017.

[21] D. Saintillan, "Nonlinear interactions in electrophoresis of ideally polarizable particles," *Phys. Fluids*, vol. 20, no. 6, p. 067104, 2008.

[22] D. House, H. Luo, and S. Chang, "Numerical study on dielectrophoretic chaining of two ellipsoidal particles," *J. Colloid Interf. Sci*, vol. 374, no. 1, pp. 141 – 149, 2012.

[23] M. R. Hossan, R. Dillon, A. K. Roy, and P. Dutta, "Modeling and simulation of dielectrophoretic particle-particle interactions and assembly," *J. Colloid Interface Sci.*, vol. 394, pp. 619–629, 2013.

[24] S. Kang, "Dielectrophoretic motions of a pair of particles in the vicinity of a planar wall under a direct-current electric field," *Journal of Electrostatics*, vol. 89, pp. 30–41, 2017.

[25] H. J. Keh and S. B. Chen, "Electrophoresis of a colloidal sphere parallel to a dielectric plane," *J. Fluid Mech.*, vol. 194, pp. 37–390, 1988.

[26] E. Yariv and H. Brenner, "Near-contact electrophoretic motion of a sphere parallel to a planar wall," *J.Fluid Mech.*, vol. 484, pp. 85–111, 2003.

[27] W. D. Ristenpart, I. A. Aksay, and D. A. Saville, "Electrically driven flow near a colloidal particle close to an electrode with a faradaic current," *Langmuir*, vol. 23, pp. 4071–4080, 03 2007.

[28] W. D. Ristenpart, I. A. Aksay, and D. A. Saville, "Electrohydrodynamic flow around a colloidal particle near an electrode with an oscillating potential," *J. Fluid. Mech.*, vol. 575, pp. 83–109, 2007.

[29] E. Yariv, "Electro-hydrodynamic particle levitation on electrodes," *J. Fluid Mech.*, vol. 645, pp. 187–210, 2010.

[30] H. J. Keh, K. D. Horng, and J. Kuo, "Boundary effects on electrophoresis of colloidal cylinders," *J. Fluid Mech.*, vol. 231, pp. 211–228, 1991.

[31] L. J. Wang and H. J. Keh, "Electrophoretic motion of a colloidal cylinder near a plane wall," *Microfluid. and Nanofluid.*, vol. 10, no. 1, pp. 81–95, 2011.

[32] S. A. Guelcher, Y. Solomentsev, and J. L. Anderson, "Aggregation of pairs of particles on electrodes during electrophoretic deposition," *Powder Technol.*, vol. 110, no. 1, pp. 90–97, 2000.

[33] J. A. Fagan, P. J. Sides, and D. C. Prieve, "Vertical motion of a charged colloidal particle near an ac polarized electrode with a nonuniform potential distribution: Theory and experimental evidence," *Langmuir*, vol. 20, pp. 4823–4834, 06 2004.

[34] J. A. Fagan, P. J. Sides, and D. C. Prieve, "Mechanism of rectified lateral motion of particles near electrodes in alternating electric fields below 1 khz," *Langmuir*, vol. 22, pp. 9846–9852, 11 2006.

[35] Y. Solomentsev, M. Bevan, and J. L. Anderson, "Aggregation dynamics for two particles during electrophoretic deposition under steady fields," *Langmuir*, vol. 16, pp. 9208–9216, 11 2000.

[36] K. H. Kang, X. Xuan, Y. Kang, and D. Li, "Effects of DC-dielectrophoretic force on particle trajectories in microchannels," *J. Applied Physics*, vol. 99, no. 064702, pp. 1–8, 2006.

[37] B. Cetin and D. Li, "Lab-on-a-chip device for continuous particle and cell separation based on electrical properties via AC-dielectrophoresis," *Electrophoresis*, vol. 31, pp. 3035–3043, 2010.

[38] S. Büyükkoçak, M. B. Özer, and B. Çetin, "Numerical modeling of ultrasonic particle manipulation for microfluidic applications," *Microfluid. Nanofluid.*, vol. 17, no. 6, pp. 1025–1037, 2014.

[39] C. E. B. S. Cetin B, Ozer MB, "An integrated acoustic and dielectrophoretic particle manipulation in a microfluidic device for particle wash and separation fabricated by mechanical machining," *Biomiccrofluidics*, vol. 10, no. 1, p. 8, 2016.

[40] M. A. Şahin, B. Çetin, and M. B. Özer, "Investigation of effect of design and operating parameters on acoustophoretic particle separation via 3D device-level simulations," *Microfluidics and Nanofluidics*, vol. 24, no. 1, p. 8, 2019.

[41] B. Cetin, S. Buyukkocak, S. Zeinali, and B. Ozer, "Simulation of an integrated microfluidic device for bioparticle wash, separation and concentration," in *ASME 4th International Conference on Micro/Nanoscale Heat and Mass Transfer*, no. 22181, 11–14 December 2013.

[42] C. Y. Chan, A. N. Beris, and S. G. Advani, "Second-order boundary element method calculations of hydrodynamic interactions between particles in close proximity," *Int. J. Numer. Methods Fluids*, vol. 14, no. 9, pp. 1063–1086, 1992.

[43] L. G. Leal, *Advanced Transport Phenomena: Fluid Mechanics and Convective Transport Processes*, pp. 430–434. Artech House, 2006.

[44] H. Ohshima and A. Hyono, "Electrostatic interaction between two cylindrical soft particles," *Journal of Colloid and Interface Science*, vol. 333, no. 1, pp. 202–208, 2009.

[45] M. B. Ranade, "Adhesion and removal of fine particles on surfaces," *Aerosol Science and Technology*, vol. 7, no. 2, pp. 161–176, 1987.

[46] H. J. Keh and J. L. Anderson, "Boundary effects on electrophoretic motion of colloidal spheres," *J. Fluid Mech.*, vol. 153, pp. 417–439, 1985.

[47] D. Saintillan, "Nonlinear interactions in electrophoresis of ideally polarizable particles," *Phys. Fluids*, vol. 20, no. 067104, 2008.

[48] O. Nicotra, A. L. Magna, and S. Coffa, "Particle-chain formation in a dc dielectrophoretic trap; a reaction-diffusion approach," *J. Applied Physics*, vol. 95, no. 073702, 2009.

[49] L. H. House DL, "Effect of direct current dielectrophoresis on the trajectory of a non-conducting colloidal sphere in a bent pore," *Electrophoresis.*

[50] C. S. House DL, Luo H, "Numerical study on dielectrophoretic chaining of two ellipsoidal particles.," *J Colloid Interface Sci.*

[51] *Numerical Investigation of DC Dielectrophoretic Particle Transport*, vol. Volume 2, Fora: Cavitation and Multiphase Flow; Fluid Measurements and Instrumentation; Microfluidics; Multiphase Flows: Work in Progress; Fluid-Particle Interactions in Turbulence of *Fluids Engineering Division Summer Meeting*, 08 2014. V002T19A004.

[52] S. Kang, "Dielectrophoretic motions of multiple particles under an alternating-current electric field," *Eur. J. Mech. B-Fluid*, vol. 54, pp. 53–68, 2015.

[53] D. L. House and H. Luo, "Electrophoretic mobility of a colloidal cylinder between two parallel walls," *Eng. Anal. Bound. Elem.*, vol. 34, no. 5, pp. 471 – 476, 2010.

[54] A. Ben Richou, A. Ambari, M. Lebey, and J. Naciri, "Drag force on a circular cylinder midway between two parallel plates at re $<$ 1 part 2: moving uniformly (numerical and experimental)," *Chemical Engineering Science*, vol. 60, no. 10, pp. 2535–2543, 2005.

[55] L. C. Wrobel, *The Boundar Element Method, Volume 1, Applications in Thermo-Fluids and Acoustics*, pp. 295–296. John Wiley & Sons, 2002.

[56] L. Gaul, M. Kögl, and M. Wagner, "Boundary element methods for engineers and scientists: An introductory course with advanced topics," *Appl. Mech. Rev.*, vol. 57, no. 6, pp. B31–B31, 2004.

[57] S. Zeinali, B. Cetin, S. Oliaei, and Y. Karpat, "Fabrication of continuous flow microfluidic device with 3D electrode structures for high throughput DEP applications using mechanical machining," *Electrophoresis*, vol. 36, pp. 1432–1442, 2015.

[58] Z. Karakaya, B. Baranoglu, B. Cetin, and A. Yazici, "A parallel boundary element formulation for tracking multiple particle trajectories in Stoke's flow for microfluidic applications," *CMES-Computer Modeling in Engineering and Science*, vol. 104, pp. 227–249, 2015.

[59] D. J. Jefferey and Y. Onishi, "The Slow Motion of a Cylinder Next to a Plane Wall," *The Quarterly Journal of Mechanics and Applied Mathematics*, vol. 34, pp. 129–137, 05 1981.

[60] D. L. House, *Applications of the Boundary Element Method of the Boundary Element Method for Electrokinetics in Microfluidics*. Phd dissertation, Vanderbilt University, 2012.

[61] J. C. F. Telles, "A self-adaptive co-ordinate transformation for efficient numerical evaluation of general boundary element integrals," *International Journal for Numerical Methods in Engineering*, vol. 24, no. 5, pp. 959–973, 1987.

[62] W. D. Ristenpart, I. A. Aksay, and D. A. Saville, "Electrically driven flow near a colloidal particle close to an electrode with a faradaic current," *Langmuir*, vol. 23, no. 7, pp. 4071–4080, 2007.

Appendix A

Calculation of DEP Force

In order to find the resulting DEP force on the particle, Maxwell Stress Tensor (MST), σ_{MST}, has to be integrated over the particle boundary as follows:

$$\mathbf{F} = \oint_{\partial\mathcal{D}} \boldsymbol{\sigma}_{\mathrm{MST}} \cdot \mathbf{n} \, d\Gamma \tag{A.1}$$

Maxwell Stress Tensor is defined to be,

$$\sigma_{\mathrm{MST}} = \varepsilon \mathbf{E} \otimes \mathbf{E} - \frac{1}{2}\varepsilon(\mathbf{E} \cdot \mathbf{E}) \, \mathbf{I} \tag{A.2}$$

where the symbol $\otimes$ represents the dyadic product. Let $\mathbf{a}$ and $\mathbf{b}$ be two vectors in the following form:

$$\mathbf{a} = \begin{bmatrix} \mathrm{a_x} \\ \mathrm{a_y} \\ \mathrm{a_z} \end{bmatrix} \quad \text{and} \quad \mathbf{b} = \begin{bmatrix} \mathrm{b_x} \\ \mathrm{b_y} \\ \mathrm{b_z} \end{bmatrix}, \tag{A.3}$$

then dyadic product is defined as follows:

$$\mathbf{a} \otimes \mathbf{b} \stackrel{\mathrm{def}}{=} \begin{bmatrix} \mathrm{a_x b_x} & \mathrm{a_x b_y} & \mathrm{a_x b_z} \\ \mathrm{a_y b_x} & \mathrm{a_y b_y} & \mathrm{a_y b_z} \\ \mathrm{a_z b_x} & \mathrm{a_z b_y} & \mathrm{a_z b_z} \end{bmatrix}. \tag{A.4}$$

Provided that **a** and **b** are two vectors in the following form. $\mathrm{a} = [\mathrm{a}_1, \mathrm{a}_2, \ldots, \mathrm{a}_\mathrm{n}]$ and $\mathrm{b} = [\mathrm{b}_1, \mathrm{b}_2, \ldots, \mathrm{b}_\mathrm{n}]$ their dot product, $\mathbf{a} \cdot \mathbf{b}$, is defined as

$$\mathbf{a} \cdot \mathbf{b} = \sum_{i=1}^{n} \mathrm{a_i b_i} = \mathrm{a}_1\mathrm{b}_1 + \mathrm{a}_2\mathrm{b}_2 + \cdots + \mathrm{a}_\mathrm{n}\mathrm{b}_\mathrm{n} \tag{A.5}$$

For a 2-D electric field, MST becomes:

$$\sigma_{\mathrm{MST}} = \varepsilon \begin{bmatrix} \mathrm{E_x^2} & \mathrm{E_x E_y} \\ \mathrm{E_x E_y} & \mathrm{E_y^2} \end{bmatrix} - \frac{1}{2} \begin{bmatrix} \mathrm{E_x^2 + E_y^2} & 0 \\ 0 & \mathrm{E_x^2 + E_y^2} \end{bmatrix} \tag{A.6}$$

Therefore x and y components of the forces become:

$$\mathbf{F_x} = \oint_{\partial\mathcal{D}} \varepsilon \left[\left(\frac{\mathrm{E_x^2}}{2} - \frac{\mathrm{E_y^2}}{2} \right) \mathrm{n_x} + \mathrm{E_x E_y n_y} \right] \mathrm{d}\Gamma \tag{A.7}$$

$$\mathbf{F_y} = \oint_{\partial\mathcal{D}} \varepsilon \left[\mathrm{E_x E_y n_x} + \left(\frac{\mathrm{E_y^2}}{2} - \frac{\mathrm{E_y^2}}{2} \right) \mathrm{n_y} \right] \mathrm{d}\Gamma \tag{A.8}$$

where

$$\varepsilon = \varepsilon_0 \cdot \varepsilon_r \tag{A.9}$$

and the value of the $\varepsilon_0 = 8.8542\mathrm{e}^{-12}$ $[\mathrm{C^2N^{-1}m^{-2}}]$ and ε_r=80

Appendix B

Evaluation of Singular Integrals

A singular integral is one that reaches to an infinite value within its domain of integration. Once applied to singular integrals, regular Gauss quadrature yields inaccurate results. There are various integration techniques that overcome these problems such as weighted gaussian integration, singularity subtraction technique, element subdivision technique [55]. In this work, due to its computational efficiency and ease of implementation, *a self-adaptive co-ordinate transformation for efficient numerical evaluation for boundary element integrals* by Telles [61] is employed.

Let us assume that there exists an integral:

$$I = \int_{-1}^{1} f(\eta) d\eta \tag{B.1}$$

where f(η) is singular at a point $\bar{\eta}$. In this method, there exists a non-linear transformation which is always true without any partition for any type of singularity. If one chooses a third order relation for η such that:

$$\eta = a\gamma^3 + b\gamma^2 + c\gamma + d \tag{B.2}$$

coefficients of such transformation become:

$$a = 1/Q \tag{B.3}$$

$$b = -3\bar{\gamma}/Q \tag{B.4}$$

$$c = 3\bar{\gamma}^2/Q \tag{B.5}$$

$$d = -b \tag{B.6}$$

$$Q = 1 + 3\bar{\gamma}^2 \tag{B.7}$$

where $\bar{\gamma}$ is the value of γ which satisfies $\eta(\bar{\gamma}) = \bar{\eta}$. Such a parameter is given by:

$$\gamma = \sqrt[3]{(\eta\eta^* + |\eta^*|)} + \sqrt[3]{(\eta\eta^* - |\eta^*|)} + \bar{\eta} \tag{B.8}$$

where $\eta^* = \bar{\eta}^2 - 1$. Thus, equation B.1 becomes:

$$\int_{-1}^{1} f\{[(\gamma - \bar{\gamma})^3 + \bar{\gamma}(\bar{\gamma}^2 + 3)]/(1 + 3\bar{\gamma})^2\}3(\gamma - \bar{\gamma})^2/(1 + 3\bar{\gamma}^2)\mathrm{d}\gamma \tag{B.9}$$

This transformation aims to introduce a Jacobian such that rate of change of Jacobian of transformation cancels out rate of change of Green's function approaching to infinity. In Fig. B.1, the non-uniform order of the gauss points due to transformation shown in equation B.8 is seen.

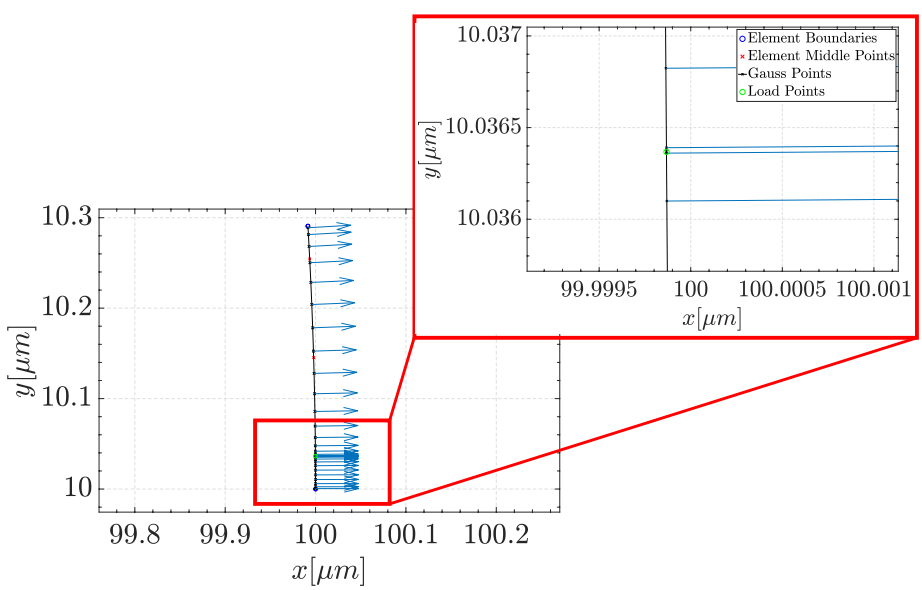

Figure B.1: Non-uniform transformation of Gauss points on the particle boundary for a singular integral

Appendix C

Boundary Conditions

C.1 Conducting Wall

Due to presence of EDL, electrical boundary condition on the particle is a homogenous Neuman boundary condition:

$$\mathbf{n} \cdot \nabla\phi = 0 \tag{C.1}$$

$$\nabla\phi = \nabla\phi^{\mathrm{D}} + \nabla\phi^{\infty} \tag{C.2}$$

$$\mathbf{n} \cdot \nabla\phi^{\mathrm{D}} = \mathbf{n} \cdot \nabla\phi - \mathbf{n} \cdot \nabla\phi^{\infty} \tag{C.3}$$

note that $\mathbf{n} \cdot \nabla\phi = 0$ due to boundary condition shown in equation C.1. Thus,

$$\mathbf{n} \cdot \nabla\phi^{\mathrm{D}} = -\mathbf{n} \cdot \nabla\phi^{\infty} = \mathrm{n_y E^{\infty}} \tag{C.4}$$

provided that the electric field is in y direction. As for the Stoke's boundary conditions, slip boundary conditions on the particle become:

$$\mathbf{u}_{\mathrm{p}}^{\mathrm{S}} = \frac{\varepsilon_m \zeta_{\mathrm{p}}}{\mu} \left(\mathbf{I} - \mathbf{nn}\right) \cdot \nabla\phi \tag{C.5}$$

$$
\begin{aligned}
\mathbf{u}_{\mathrm{p}}^{\mathrm{S}} = & \frac{\varepsilon_m \zeta_{\mathrm{p}}}{\mu} \left(\begin{bmatrix} 1 & 0 \\ 0 & 1 \end{bmatrix} - \begin{bmatrix} \mathrm{n_x^2} & \mathrm{n_x n_y} \\ -\mathrm{n_x n_y} & \mathrm{n_y^2} \end{bmatrix} \right) \begin{bmatrix} \dfrac{\partial \phi^{\mathrm{D}}}{\partial \mathrm{x}} \\ \dfrac{\partial \phi^{\mathrm{D}}}{\partial \mathrm{y}} \end{bmatrix} \\
& + \frac{\varepsilon_m \zeta_{\mathrm{p}}}{\mu} \left(\begin{bmatrix} 1 & 0 \\ 0 & 1 \end{bmatrix} - \begin{bmatrix} \mathrm{n_x^2} & \mathrm{n_x n_y} \\ -\mathrm{n_x n_y} & \mathrm{n_y^2} \end{bmatrix} \right) \begin{bmatrix} 0 \\ -\mathrm{E}^{\infty} \end{bmatrix}
\end{aligned} \tag{C.6}
$$

Final expression for the boundary condition on the particle becomes:

$$
\begin{aligned}
\mathbf{u}_{\mathrm{p}}^{\mathrm{S}} = & -\frac{\varepsilon_m \zeta_{\mathrm{p}}}{\mu} \begin{bmatrix} -\left(1-\mathrm{n_x^2}\right) \dfrac{\partial \phi^{\mathrm{D}}}{\partial \mathrm{x}} + \dfrac{\partial \phi^{\mathrm{D}}}{\partial \mathrm{y}} \mathrm{n_x n_y} - \mathrm{n_x n_y E}^{\infty} \\ \mathrm{n_x n_y} \dfrac{\partial \phi^{\mathrm{D}}}{\partial \mathrm{x}} - \left(1-\mathrm{n_y^2}\right) \dfrac{\partial \phi^{\mathrm{D}}}{\partial \mathrm{y}} + \left(1-\mathrm{n_y^2}\right) \mathrm{E}^{\infty} \end{bmatrix} \\
= & -\frac{\varepsilon_m \zeta_{\mathrm{p}}}{\mu} \begin{bmatrix} \mathrm{E_t t_x} - \mathrm{n_x n_y E}^{\infty} \\ \mathrm{E_t t_y} + \left(1-\mathrm{n_y^2}\right) \mathrm{E}^{\infty} \end{bmatrix}
\end{aligned} \tag{C.7}
$$

Regarding the slip velocity on the wall, in order to obtain disturbance velocity the following is made:

$$
\mathbf{u}^{\mathrm{D}} = \mathbf{u}^{\mathrm{S}} - \mathbf{u}^{\infty} \tag{C.8}
$$

As a result,

$$
\mathbf{u}^{\mathrm{D}} = \frac{\varepsilon\ \zeta_{\mathrm{w}}}{\mu} \left(\mathbf{I} - \mathbf{nn}\right) \cdot \nabla \phi^{D} \tag{C.9}
$$

$$
\mathbf{u}^{\mathrm{D}} = -\frac{\varepsilon_m\ \zeta_{\mathrm{w}}}{\mu} \begin{bmatrix} \mathrm{E_t} \\ 0 \end{bmatrix} \tag{C.10}
$$

where $\mathrm{E_t}$ is the tangential electrical field on the boundaries of the domain.

C.2 Non-Conducting Wall

Due to presence of EDL, electrical boundary condition on the particle is a homogenous Neuman boundary condition:

$$
\mathbf{n} \cdot \nabla \phi = 0 \tag{C.11}
$$

$$
\nabla \phi = \nabla \phi^{\mathrm{D}} + \nabla \phi^{\infty} \tag{C.12}
$$

$$
\mathbf{n} \cdot \nabla \phi^{\mathrm{D}} = \mathbf{n} \cdot \nabla \phi - \mathbf{n} \cdot \nabla \phi^{\infty} \tag{C.13}
$$

note that $\mathbf{n} \cdot \nabla\phi = 0$ due to boundary condition shown in equation C.11. Thus,

$$\mathbf{n} \cdot \nabla\phi^{\mathrm{D}} = -\mathbf{n} \cdot \nabla\phi^{\infty} = \mathrm{n_x E^{\infty}} \tag{C.14}$$

provided that the electric field is in x− direction. As for the Stoke's boundary conditions, slip boundary conditions on the particle become:

$$\mathbf{u}_{\mathrm{p}}^{\mathrm{S}} = \frac{\varepsilon_m \zeta_{\mathrm{p}}}{\mu} \left(\mathbf{I} - \mathbf{nn}\right) \cdot \nabla\phi \tag{C.15}$$

$$\begin{aligned} \mathbf{u}_{\mathrm{p}}^{\mathrm{S}} = & \frac{\varepsilon_m \zeta_{\mathrm{p}}}{\mu} \left(\begin{bmatrix} 1 & 0 \\ 0 & 1 \end{bmatrix} - \begin{bmatrix} \mathrm{n_x^2} & \mathrm{n_x n_y} \\ -\mathrm{n_x n_y} & \mathrm{n_y^2} \end{bmatrix} \right) \begin{bmatrix} \dfrac{\partial\phi^{\mathrm{D}}}{\partial \mathrm{x}} \\ \dfrac{\partial\phi^{\mathrm{D}}}{\partial \mathrm{y}} \end{bmatrix} \\ & + \frac{\varepsilon_m \zeta_{\mathrm{p}}}{\mu} \left(\begin{bmatrix} 1 & 0 \\ 0 & 1 \end{bmatrix} - \begin{bmatrix} \mathrm{n_x^2} & \mathrm{n_x n_y} \\ -\mathrm{n_x n_y} & \mathrm{n_y^2} \end{bmatrix} \right) \begin{bmatrix} \text{-E}^{\infty} \\ 0 \end{bmatrix} \end{aligned} \tag{C.16}$$

Final expression for the boundary condition on the particle becomes:

$$\begin{aligned} \mathbf{u}_{\mathrm{p}}^{\mathrm{S}} = & -\frac{\varepsilon_m \zeta_{\mathrm{p}}}{\mu} \begin{bmatrix} -\left(1 - \mathrm{n_x^2}\right) \dfrac{\partial\phi^{\mathrm{D}}}{\partial \mathrm{x}} + \dfrac{\partial\phi^{\mathrm{D}}}{\partial \mathrm{y}} \mathrm{n_x n_y} - \left(1 - \mathrm{n_x^2}\right) \mathrm{E}^{\infty} \\ \mathrm{n_x n_y} \dfrac{\partial\phi^{\mathrm{D}}}{\partial \mathrm{x}} - \left(1 - \mathrm{n_y^2}\right) \dfrac{\partial\phi^{\mathrm{D}}}{\partial \mathrm{y}} + \mathrm{n_x n_y E}^{\infty} \end{bmatrix} \\ = & -\frac{\varepsilon_m \zeta_{\mathrm{p}}}{\mu} \begin{bmatrix} \mathrm{E_t t_x} - \left(1 - \mathrm{n_x^2}\right) \mathrm{E}^{\infty} \\ \mathrm{E_t t_y} + \mathrm{n_x n_y E}^{\infty} \end{bmatrix} \end{aligned} \tag{C.17}$$

Regarding the slip velocity on the wall, in order to obtain disturbance velocity the following is made:

$$\mathbf{u}^{\mathrm{D}} = \mathbf{u}^{\mathrm{S}} - \mathbf{u}^{\infty} \tag{C.18}$$

As a result,

$$\mathbf{u}^{\mathrm{D}} = \frac{\varepsilon\ \zeta_{\mathrm{w}}}{\mu} \left(\mathbf{I} - \mathbf{nn}\right) \cdot \nabla\phi^{D} \tag{C.19}$$

$$\mathbf{u}^{\mathrm{D}} = -\frac{\varepsilon_m\ \zeta_{\mathrm{w}}}{\mu} \begin{bmatrix} \mathrm{E_t} \\ 0 \end{bmatrix} \tag{C.20}$$

where $\mathrm{E_t}$ is the tangential electrical field on the boundaries of the domain.

Appendix D

Convergence of the Solver

Throughout the simulations, quadratic elements are utilized to approximate both field variables on elements and approximate geometric entities throughout the computations. As a result, log-log error graph as a function of number of elements used the problem presented in section 3.2.1 is drawn.

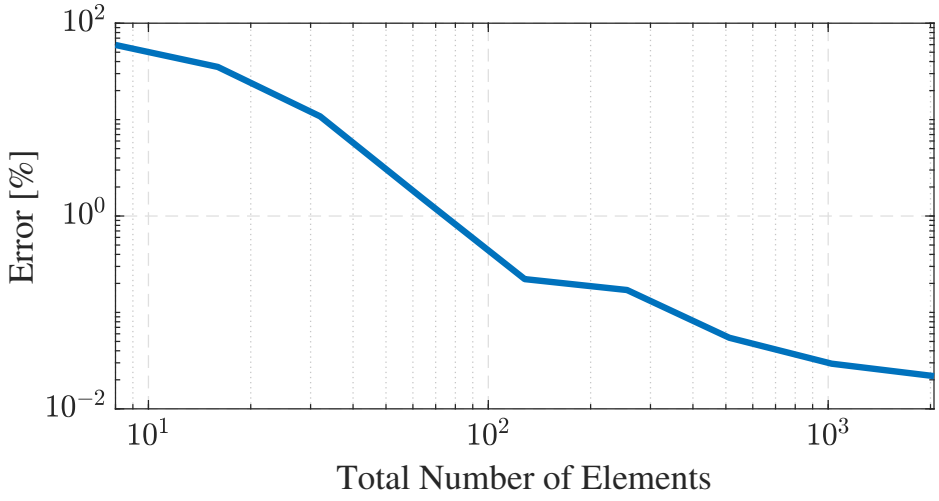

Figure D.1: Convergence of the quadratic solver

Appendix E

Code

```
        clear ; clc ; close all;
%% Current Parameters
tic
% Starting Location
StartAt = 15e-06-7.5e-06;
RatWall = [ 1/250;
            1/1];

 Nch_ve_Ninc =  [  360;  % Nx
                  36*3];

%  % Remeshing Parameters at Horizontal and Vertical
    Distances
 Lambda  = [501] * 1e09;

% Last Two Are Horizontal Distance
NoOfHor = 0;
VerNo = length(Lambda) - NoOfHor;
LambdaCounter = 1;

```

```
% Check whether This is  a First Run or Not
IlkFlag = true;

% Save Every How many Data?
SaveEvery = 2;

% ***********************************************
%                          Time Related Variables
% ***********************************************
Time.dt       = 8e-02;
Time.time_f = 50000;
Time.Ntime   =  Time.time_f/Time.dt;

beautify;
% ************************************************
%                              MESH GENERATION
% ************************************************
CG.pos = zeros(2,3,1); CG.Pos_update(1:2,1:3,1) = 0; CG.time = 1;
[Geom,Mat,Mesh,CG] = Input_Channel_Inclusions_v00_Circular(StartAt,LambdaCounter,Nch_ve_Ninc,CG,IlkFlag,RatWall);

CG.pos(:,3,1) = 0;

% Data Save Counter AND various Flags
Counter = 0 ; Counter2 = 0; YouShallContinue = 1; AreWeIn = 0; Flaag = 1; ShallISave = true; PostProcVar.Creation = true;

PostProcVar.Zeta_inc = Mat.ZP_inc;
PostProcVar.Zeta_w = Mat.ZP_w;

%************************************************
```

```
%          G00 & H00 MATRICES FOR STOKES and Laplace
%*************************************************
LambdaCounter = 1; t = 1; close all;

while YouShallContinue == true
    Time.dtAll(t) = Time.dt;
    DistBetw =  CG.pos(2,1,t) - CG.pos(1,1,t);
    DistBetwy = (CG.pos(2,2,t) - CG.pos(1,2,t));
    fprintf('Distance Between Particles in x %.3f\n',(DistBetw)*1E9);
    fprintf('Distance Between Particles in y %.3f\n',(DistBetwy)*1E9);
    VerticalDistance =  ( CG.pos(1,2,t) - 5e-06);
    fprintf('Starting point of Center of Lowest point \n (y dir): %.5f nm\n',min(Mesh.XM(Mesh.NchNodes+1:end,2))*1e9);

    NewLambd =    min(Mesh.XM(Mesh.NchNodes+1:end,2))*1e9;
    PostProcVar.L_Ninc(LambdaCounter,:) = [max(Mesh.ELength(Geom.Nch+1:end,1)) min(Mesh.ELength(Geom.Nch+1:end,1))]*1e9;
    PostProcVar.L_Nch(LambdaCounter,:)  = [max(Mesh.ELength(1:Geom.Nch,1))      min(Mesh.ELength(1:Geom.Nch,1))]*1e9;

    %% Remeshing Check Vertical Distance
        if LambdaCounter <= VerNo && LambdaCounter <= length(Lambda) && NewLambd <= Lambda(LambdaCounter)*1e9
            fprintf('--*-*-*-*Entered Remeshing Vertical.--*-*-*-*\n')
            IlkFlag = false;
            % ****************************************
```

```
%      MESH GENERATION
% ****************************************
[Geom,Mat,Mesh,CG] = Input_Channel_Inclusions_v00_Circular(NewLambd,LambdaCounter,Nch_ve_Ninc,CG,IlkFlag,RatWall);

% ****************************************
%  G00 & H00 Matrice FOR Stokes and Laplace
%****************************************

funcs1 = {@BEMStokes_Assembly_Circular, @BEMLaplace_Assembly_Circular};

arguments1 = {'C','C',Geom,Mat,Mesh,CG;
              Geom,Mat,Mesh,CG,'C','C'};

solutions3 = cell(1,2);  solutions4 = cell(1,2);

parfor ii = 1:2
    [solutions3{ii},solutions4{ii}] = funcs1{ii}(arguments1{ii,:});
end

HH.Stokes.OO = solutions3{1,1};     HH11 = solutions3{1,2} ;
GG.Stokes.OO = solutions4{1,1};     GG11 = solutions4{1,2} ;

disp('Done S_00 and L_00')
GG.Stokes.invOO = pinv(GG.Stokes.OO);
disp('*******************************')
```

```
            fprintf('Nx = %.2f,  Ninc = %.2f\n',Nch_ve_Ninc(1,LambdaCounter),Nch_ve_Ninc(2,LambdaCounter));
            disp('*******************************')
            LambdaCounter = LambdaCounter + 1  ;


%% Remeshing Check Horizontal Distance
    elseif LambdaCounter > VerNo && LambdaCounter <= length(Lambda)  && DistBetw <= Lambda(LambdaCounter)
        fprintf('--*-*-*-*Entered Remeshing- Horizontal.--*-*-*-*\n')
        IlkFlag = false;
        % ********************************************
        %                          MESH GENERATION
        % ********************************************
        [Geom,Mat,Mesh,CG] = Input_Channel_Inclusions_v00_Circular(NewLambd,LambdaCounter,Nch_ve_Ninc,CG,IlkFlag,RatWall);

        % ********************************************
        %                    G00 & H00 MATRICES FOR STOKES and Laplace
        %*******************************************

        funcs1 = {@BEMStokes_Assembly_Circular,@BEMLaplace_Assembly_Circular};

        arguments1 = {'C','C',Geom,Mat,Mesh,CG;
                      Geom,Mat,Mesh,CG,'C','C'};

        solutions3 = cell(1,2);  solutions4 = cell(1,2);
```

```
        parfor ii = 1:2
            [solutions3{ii},solutions4{ii}] = funcs1{ii}(arguments1{ii,:});
        end

        HH.Stokes.OO = solutions3{1,1};  HH11 = solutions3{1,2} ;
        GG.Stokes.OO = solutions4{1,1};  GG11 = solutions4{1,2} ;

        disp('Done S_00 and L_00')
        GG.Stokes.invOO = pinv(GG.Stokes.OO);
        disp('************************************')
        fprintf('Nx = %.2f, Ninc = %.2f\n',Nch_ve_Ninc(1,LambdaCounter),Nch_ve_Ninc(2,LambdaCounter));
        disp('************************************')
        LambdaCounter = LambdaCounter + 1 ;

        end
    %% Continue After Remesh Solve for H and G Matrices for Stokes and Laplace
    % Start Parralel Process
    funcs1 = {@BEMLaplace_Assembly_Circular, @BEMLaplace_Assembly_Circular, @BEMLaplace_Assembly_Circular,...
        @BEMStokes_Assembly_Circular, @BEMStokes_Assembly_Circular, @BEMStokes_Assembly_Circular};

    arguments1 = {Geom,Mat,Mesh,CG,'C','P';
        Geom,Mat,Mesh,CG,'P','C';
        Geom,Mat,Mesh,CG,'P','P';
```

```
        'C', 'P',Geom,Mat,Mesh,CG;
        'P', 'C',Geom,Mat,Mesh,CG;
        'P', 'P',Geom,Mat,Mesh,CG};

    solutions1 = cell(1,2); solutions2 = cell(1,2);

    parfor ii = 1:6
        [solutions1{ii}, solutions2{ii}] = funcs1{ii}(
            arguments1{ii,:});
    end

    solutions1  = solutions1';
    solutions2  = solutions2';

    HH.Stokes.OP = solutions1{4,1};   GG.Stokes.OP =
        solutions2{4,1};
    HH.Stokes.PO = solutions1{5,1};   GG.Stokes.PO =
        solutions2{5,1};
    HH.Stokes.PP = solutions1{6,1};   GG.Stokes.PP =
        solutions2{6,1};
    GG.Laplace = [solutions4{1,2}  solutions2{1,1};
        solutions2{2,1} solutions2{3,1}];
    HH.Laplace = [solutions3{1,2}  solutions1{1,1};
        solutions1{2,1} solutions1{3,1}];

    clear solutions1; clear solutions2;

    %% Continue the Process Consecutively
    [GG.Laplace,HH.Laplace] = BEMLaplace_BCImplementation(
        Geom,Mesh,GG,HH);
    disp('Stokes & Laplace H and G Done.');

    % ****************************************
```

```
%        SOLUTION OF LAPLACE & MST CALCULATION
% ****************************************

x_L = BEM_Solver(Mesh.BC.Laplace(:,2),GG.Laplace,HH.Laplace);

[Solution.Laplace.Phi,Solution.Laplace.En,Solution.Laplace.Et] = ...
    BEM_GetUQQt(Geom,Mat,Mesh,x_L,CG);

[GG,HH,Mesh] = ...
    BEMStokes_BCImplementation_With_Slip_NewBCFormulation(Geom,Mat,Mesh,Solution,GG,HH);

if t > 1
    if ShallISave == true
        u_BPrev = u_B;
        MeshPrev = Mesh;

    end

else
    u_BPrev = 0;

end

 f_EK = EK_Force_and_Torque_Calculation(Geom,Mat,Mesh,CG,Solution);

%% Enter Impedance Formulation Check Error Conditions and Reiterate if Necessary
```

```
[u_B,u_BPrev,Counter,Counter2,PostProcVar,t,Time,Geom,Mesh,CG,Flaag,LambdaCounter,Lambda,Nch_ve_Ninc,ShallISave,SaveEvery]...
    = Impedance_FormulationSedimentation(t,u_BPrev,Time,Geom,Mesh,GG,HH,f_EK,CG,Mat,SaveEvery,Counter,Counter2,PostProcVar,Flaag,LambdaCounter,Lambda,Nch_ve_Ninc,ShallISave);

%% Move Forward in Time if Everyting is Good
if ShallISave == true

    for i = 1:Geom.Ni

        Time.dtAll(t) = Time.dt;
        dummy = sprintf('u_B (%1d) = %3.8f[um/s] %3.8f[um/s] %1.1f[degree/s] \n',...
            [i u_B(i,1)*1e6 u_B(i,2)*1e6 u_B(i,3)*180/pi]);
        disp(dummy);
        angle = CG.pos(i,3,t+1)*180/pi;
        dummy = sprintf('Pos (%1d) = %3.3f[um] %3.3f[um] %3.1f%c\n',...
            [i CG.pos(i,1,t+1)*1e6 CG.pos(i,2,t+1)*1e6 mod(angle,360) char(176)]);
        disp(dummy)
    end

    disp('
        ')
    disp(' ')

```

```
        dummy = sprintf('Time = %2.3f\n', sum(Time.dtAll(1:t)));
        disp(dummy);

        if mod(t,10) == 0   &&  ShallISave
            save('Kurtarma.mat','-v7.3');

        elseif DistBetw <= 200e-09 && Flaag == 1 && ShallISave
            save('KurtarmaOzel_100.mat','-v7.3');
            Flaag = 0 ;
        end


        t = t + 1;
        CG.time = t;
    else
        CG.KaydetsinMi = ShallISave;
        [Mesh,CG] = Moving_Inclusion_Mesh_UpdateV2(t,Geom,Mesh,CG);

        for i = 1:Geom.Ni
            dummy = sprintf('u_B (%1d) = %3.8f[um/s] %3.8f[um/s] %1.1f[degree/s] \n',...
                [i u_B(i,1)*1e6 u_B(i,2)*1e6 u_B(i,3)*180/pi]);
        end

        disp('------------------------------------------------------------------------------------------------------------')
        fprintf('Restarting Process!!!!!\n')

```

```
    end

    save PostProcVar PostProcVar;
    save Time Time;



end
%%
 lambda = Geom.R_inc(1,1)/(CG.pos(1,2,t-1));
Psi_Zero = asech(lambda);
Mu_inc = Mat.em * Mat.ZP_inc(1)/ Mat.mu ;
Mu_w = Mat.em * Mat.ZP_w/Mat.mu;
Uxx =  coth(2*Psi_Zero);
YouShallContinue = false;
U_hat = u_B(1)/((-Mu_w+Mu_inc(1))*Mesh.Einf);
Omega_hat = u_B(3)*Mat.mu(1)*Geom.R_inc(1)/Mat.em/(Mat.
    ZP_inc(1)-Mat.ZP_w)/Mesh.Einf;
OmegaRot = sech(Psi_Zero)/sinh(2*Psi_Zero);
ErrorBen = (U_hat-Uxx)/(Uxx)*1e2
ErRotBen = (Omega_hat-OmegaRot)/(OmegaRot)*1e2
```